

# Fermi National Accelerator Laboratory

FERMILAB-Pub-87/176-E

[E-741/CDF]

## Cosmic Ray Test of the CDF Central Calorimeters\*

R. G. Wagner

Argonne National Laboratory  
Argonne, Illinois 60439, USA

S. Mikamo

National Laboratory for High Energy Physics, KEK  
Oho, Tsukuba, Ibaraki 305, Japan

S. Kobayashi and A. Murakami

Physics Department, Saga University  
Honjo, Saga 840, Japan

T. Kamon<sup>\*)</sup> and A. Yamashita

Institute of Physics, University of Tsukuba  
Sakura, Niihari, Ibaraki 305, Japan

A. Di Virgilio<sup>\*\*)</sup>

Physics Department, Purdue University  
West Lafayette, Indiana 47907, USA

D. F. Connor, S. R. Hahn, and M. R. Miller

Physics Department, University of Pennsylvania  
Philadelphia, Pennsylvania 19104, USA

J. E. Elias, E. Focardi<sup>\*\*)</sup>, and K. Yasuoka

Fermi National Accelerator Laboratory  
Batavia, Illinois 60510, USA

S. Cihangir<sup>\*)</sup>

Physics Department, University of Illinois  
Urbana, Illinois 61801, USA

July-August 1987

\* Submitted to Nucl. Instrum. Methods A



## COSMIC RAY TEST OF THE CDF CENTRAL CALORIMETERS

R.G. Wagner  
Argonne National Laboratory  
Argonne, Illinois 60439, USA

S. Mikamo  
National Laboratory for High Energy Physics, KEK  
Oho, Tsukuba, Ibaraki 305, Japan

S. Kobayashi and A. Murakami  
Physics Department, Saga University  
Honjo, Saga 840, Japan

T. Kamon \*) and A. Yamashita  
Institute of Physics, University of Tsukuba  
Sakura, Niihari, Ibaraki 305, Japan

A. Di Virgilio\*\*)   
Physics Department, Purdue University  
West Lafayette, Indiana 47907, USA

D.F. Connor, S.R. Hahn and M.R. Miller  
Physics Department, University of Pennsylvania  
Philadelphia, Pennsylvania 19104, USA

J.E. Elias, E. Focardi \*\*) and K. Yasuoka  
Fermi National Accelerator Laboratory  
Batavia, Illinois 60510, USA

S. Cihangir \*)  
Physics Department, University of Illinois  
Urbana, Illinois 61801, USA

### ABSTRACT

Measurements of the cosmic ray response of the CDF central calorimeters have been performed. For the electromagnetic calorimeter, fine grained response maps were obtained for 46 modules, and the similarity of the individual maps has been studied. For the hadron calorimeter, several basic parameters were calibrated with the use of minimum ionizing particles. In both cases the correspondence between cosmic ray results and test beam results was established.

## 1. INTRODUCTION

Cosmic ray testing of the CDF central calorimeter modules is one of a series of quality control and calibration tests performed on each of the 48 modules. These calorimeter modules span 15 degrees in azimuth and approximately 45 degrees in polar angle, and are internally subdivided into independent projective towers pointing back to the interaction region [1(a),(b) and (c)].

For the electromagnetic ( EM ) calorimeter, the principal objective of cosmic ray testing is to obtain precise response maps over the face of each tower in all 48 modules (plus 2 spares) in order to extract uniformity correction functions for the offline analysis data base. The measurements must be precise enough to achieve an overall corrected uniformity at the 1 % level as required by the CDF physics goals.

For the hadron calorimeter, the calibration of several basic characteristics of the calorimeter is performed by taking advantage of the use of minimum ionizing particles.

The mapping measurements for the EM calorimeter are made with cosmic rays because the time available for direct test beam studies is very limited, sufficient only for gain calibrations and detailed studies on a few modules (linearity, mapping etc.). Therefore, it is crucial to establish the correspondence between cosmic ray and electron responses of the calorimeter. Accurate uniformity studies were made on a small number of modules in the test beam with 50 GeV electrons to determine the applicability of the cosmic ray maps.

In addition, for both calorimeters this testing provides an important quality control function for the production line and a necessary equipment checkout function before the calorimeter modules are installed in the calibration test beam.

We present here a report on the response uniformity results for the electromagnetic (EM) calorimeter towers and some basic parameters of hadron calorimeter. The correspondence to electron test beam results and pion test beam results is also described.

Data taking began in June of 1983 following completion of the dedicated cosmic ray test stand in Industrial Building IV at Fermilab. Testing continued essentially without interruption until the last module was completed in June of 1985.

## 2. COSMIC RAY TEST STAND

### 2. 1 Introduction

In order to minimize systematic variations from module to module and allow data taking to proceed unattended for long periods of time, a dedicated cosmic ray test stand facility was constructed [2]. Functions provided by this test stand included triggering on isolated penetrating cosmic ray muons, precise tracking of the muon trajectories, computer based data acquisition and online monitoring, and gain calibrations for both the readout electronics and the calorimeter towers. The various components of the test stand are described in this section.

## 2. 2 Trigger Counters And Rates

Figure 1 shows two views of the cosmic ray test stand apparatus with a calorimeter module in place. Three planes of trigger scintillators called Upper, Lower, and Side are used to define the ten trigger roads which correspond to the ten projective towers of the calorimeter module. The scintillator pieces were cut to match the projected size of each tower individually, virtually eliminating any trigger from muons which cross tower boundaries. Two fold coincidences of either  $U_i \cdot L_i$  or  $S_i \cdot L_i$  determine the ten trigger roads where  $i$  refers to the tower number.

The spectrum of cosmic ray muons has a steep energy dependence and varies with zenith angle. The thickness of the calorimeter module is sufficient to absorb the copious soft component in cosmic rays, except for the towers near the 45 degree side. To ensure that the energy of muons satisfying the trigger requirement is in the region of minimum ionization and reduce the effects of multiple scattering and straggling, an additional 20.3 cm thick iron absorber was placed under the Lower trigger counters. Another scintillator counter plane, called Hardner, was installed below this absorber and included in the trigger requirement. Since the projective tower trigger roads are already established by the U, S, and L counters, the Hardner was implemented as two large counters for convenience.

The U, S, and L counters were cut from 7 mm thick polystyrene based scintillator and viewed by Hamamatsu type R329 phototubes. For the Hardner counters, 6.4 mm thick polystyrene scintillator was used along with RCA type 4522 phototubes. After plateauing the trigger counters, it was observed that a 50 Volt decrease in the high voltage produced no discernable effect on the trigger rates.

The total trigger rate over all ten towers including the Hardner is 1.8 Hz. Figure 2 shows the relative trigger rate for each tower obtained with the calorimeter module and the hardner in the configuration of Fig. 1. A Monte Carlo simulation result is presented with the histogram, which involves the effects of the muon energy spectrum obtained by Green et al [3] and the minimum ionization loss of muon energy in the calorimeter materials. With the extra hardner absorber in place, the minimum muon energy for triggering varies from 1.5 to 1.7 GeV across towers 0 through 5 and from 1.2 to 0.5 GeV for towers 6 to 9. From the simulation, we estimate the average energy of trigger muons to be 3.4 GeV.

### 2.3 Muon Tracking

Since the trigger roads correspond to the full size of each tower, a set of drift chambers are used to measure the trajectories of trigger muons within the more coarse roads. The upper drift chamber is actually the central muon chamber which is an integral part of the CDF calorimeter module design [4]. The side and lower drift chambers were designed and constructed specifically for the test stand. An additional constraint on the trajectory of a muon was provided by the strip chamber embedded in the EM calorimeter module at the shower maximum depth [5]. Thus, cosmic ray testing also helped to commission both the central muon chambers and the strip chamber. The fine grained spatial information provided by the chambers was useful to the data analysis in rejecting triggers caused by multiple particles.

The drift chambers consist of four layer packages containing rectangular cells running parallel to the Z-axis shown in Fig. 1, with dimensions of 6.4 cm by 2.5 cm. There are 48 cells in a package with an external cross section that is 81.3 cm wide by 10.2 cm thick. Sense wires in alternate layers are offset by 2 mm to resolve the left-right ambiguity. Operation of the chambers in limited streamer mode with a 50/50 mixture of argon and ethane (containing 1 % ethyl alcohol) provided the longitudinal coordinate using charge division on the resistive sense wires. The voltage on the cell walls was -2.5 kVolts, and that on the sense wire was +3.1 kVolts. Transverse resolutions of 250 microns on the 3.1 cm drift space and longitudinal resolutions of 4.7 cm on the 230 cm long sense wires were achieved in this test

[4]. However the longitudinal resolution is expected to be improved to better than 5 mm with a Fe-55 source calibration.

## 2. 4 Trigger And Data Acquisition Electronics

A block diagram of the cosmic ray trigger electronics is shown in Fig. 3. The ten two fold coincidences of the pairs of trigger counters  $U_i \cdot Li$  and  $S_i \cdot Li$  are made with a resolving time of 10 nsec and then summed by an OR circuit to form the basic cosmic ray signal CR. A parallel set of circuits is used to determine whether either the U plus S plane or the L plane contained multiple hits (DBLE) within 50 nsec. The single cosmic ray signal SNGL was then formed by combining CR with the Hardner counter signal (HARD) and the multiple hit veto.

To insure that cosmic ray triggers determined by the SNGL logic are not contaminated by other cosmic ray particle occurrences during the data acquisition gate live time, the presence of any late particle hits (LP) is monitored by a coincidence between SNGL and a late hit in either the U, S or L planes. This LP monitor is formed with a resolving time equal to the gate width and recorded. The final event rate was reduced from 1.8 Hz to 1.6 Hz by rejecting LP events in the offline analysis.

For each cosmic ray trigger, the data acquisition system recorded the charge from the calorimeter phototubes, the trajectory information from the muon and strip chambers, and the trigger counter hit patterns. Standard commercial CAMAC TDC, ADC, and latch modules were used to digitize the muon chamber drift time and charge division signals and to record the trigger counter pattern. For the strip chamber and phototube signals, prototype versions of the CDF front end electronics were used both to facilitate comparisons with test beam data and to avoid electronics cross normalization problems between calibration data and collider operation. In the CDF system [6], high gain-bandwidth charge integrators are followed by synchronous sample and hold buffers which are then multiplexed to a local scanning ADC in the same crate for digitization and readout for data recording. Correlated double sampling is used to remove any base line from prior signals and to reduce noise. The CDF electronics is attached to the back of each calorimeter module providing a minimum noise short interconnect environment and

eliminating the need for preamplifiers and driver/receivers to remote digitizers. A 16-bit dynamic range is provided with 11 to 33 femtoCoulombs (fC) rms noise.

When used in the collider, the basic data acquisition cycle of reset, measure, and hold for the CDF front end electronics is synchronized to the beam crossings. However, cosmic ray triggers are random occurrences which need a special synchronization in the data acquisition control logic as shown in Fig. 4. Gating cycles (reset, measure, and hold) for both the CAMAC and CDF electronics are generated by a fixed frequency oscillator and appropriate delays. A dead time flip flop allows the cycles to continue until a cosmic ray trigger occurs within the legitimate live time window of the cycle. This coincidence then sets the dead time flip flop to inhibit further cycles and freeze the event for digitization and computer readout. On completion of readout, the dead time flip flop is reset permitting gate cycles to resume until the next cosmic ray trigger. With the oscillator period set to 20 microsec, a live time window of 18 microsec was admitted corresponding to trigger efficiency of 90 %. It was essential to select CAMAC modules which provided a fast clear function to be compatible with this mode of free running gate cycles.

The data acquisition control logic also accommodated a variety of ancillary triggers by means of a CAMAC output register used as a trigger mask for selecting options. In addition to the cosmic ray trigger, the system allowed operation with LED, Xenon flash lamp, pedestal, charge injection calibration, or test triggers. Electronics checkout and system gain monitoring were automated using these options.

## 2. 5 On-line Computer And Data Recording

Data readout and on-line analysis is performed using a VAX 11/730 minicomputer. Events are logged onto magnetic tape with a standard DEC model TS-11 1600 bpi drive. All data readout is based in CAMAC using a Jorway model 411 serial branch driver. For the CDF prototype front end electronics, a special CAMAC based interface module was constructed to drive the remote scanning ADC to digitize the sample and hold values. A typical cosmic ray trigger produced approximately one hundred 16-bit words of data, so that there were about 40 K events on a tape. In addition to the event data modules, the CAMAC system contained a variety of control and

status modules to provide a complete monitoring of the test stand environment and control over the operating parameters.

The on-line main program, MIDAS [7], provides sharable images that allow the user to link the event stream to analysis routines, display and histogramming services (HBOOK/HPLOT), and data management routines (YBOS). The device drivers which service interrupts from CAMAC, readout the event data, and execute CAMAC programmed I/O commands are included in MIDAS. As a debugging aid and a tool for quick test runs or studies, a limited interactive capability was available to define, clear, and display HBOOK/HPLOT results without recompiling. This feature made remote access to the histogram data on the run in progress a convenient and much used capability.

### 3. ELECTROMAGNETIC CALORIMETER

#### 3.1 Calorimeter Description

The EM calorimeter is a stack of alternating scintillator and lead plates with one layer of strip chamber. The general description may be found in Refs [1(a)] and [1(b)]. Here we briefly describe the detector characteristics directly related to the present study.

##### 3.1.1 Scintillator, Wavelength Shifter And Phototube

The calorimeter consists of 31 scintillator plates of the type SCSN-38 [8], each 5.0 mm thick, and alternately stacked with 30 lead plates, each 1/8" thick. Light from the scintillator in each tower is collected on either side by 3 mm thick UVA acrylic wavelength shifter doped with 30 ppm Y7 [8] and is transmitted to two phototubes through UVA acrylic rods and transition pieces. The transition piece is doped with 30 ppm Y7. The phototubes are 1.5" bialkali, 10 stage HAMAMATSU R580.

The polystyrene base of scintillator is doped with two kinds of fluors, i.e. b-PBD and BDB. The wavelength of light emitted from b-PBD and BDB is about 360 nm and 430 nm respectively at the emission peak, and corresponding to a shorter (~ 10 cm) and longer (~ 100 cm) attenuation length [8]. This configuration gives rise to an increase of light output for an impact near the scintillator edge on either phototube side, causing the necessity of a uniformity study.

The Y7 wavelength shifter converts the scintillator light into light of wavelength 490 nm. The wavelength shifter response was made uniform to 3 % rms in construction of a module by a backing that was applied in areas giving a response significantly higher than the average and that suppressed the response in these regions. There is a 6 mm (air) gap between waveshifter plates servicing adjacent towers.

The tubes were "burned in" and tested at Rutgers University [9] before installation into the wedge module. Data for the dark current, quantum efficiency, gain linearity and stability were provided. The typical value of the gain and quantum efficiency is  $10^5$  and 14.4 % respectively.

### 3.1.2 Strip Chamber

The strip chamber is a wire proportional chamber located at a depth near shower maximum in the EM calorimeter [5]. The chamber covers all ten towers in a single wedge, 15 degrees in azimuth by wires and 40 to 90 degrees in polar angle by strips.

The 62 anode wires are separated by aluminum extrusion channels and ganged together in pairs except for two edge wires. The logical channel width is 14.53 mm. The wires are divided at tower 4 - 5 boundary giving a total of 64 channels. The wire numbering starts at 0 for the side of the strip chamber closest to 90 degree side and increases as X decreases, to a maximum 31. Wire number starts again on the second part of the chamber, starting at 32 for the largest X and increasing to 63 for the last wire.

The 128 cathode strips are oriented perpendicular to the wires and form the cover for the open channel extrusions containing the wires. The logical width is 16.67 mm for towers 0 to 4 (channels 0 to 68) and 20.07 mm for towers 5 to 9 (channels 69 to 127).

High voltage was fed to each logical wire channel from 4 external distribution boxes connected to a common voltage supply set at 1.5 kV. (In the present test the gain was set 2.5 times higher than nominal to be sensitive to minimum ionizing particles.) The gas is a mixture of Ar/CO<sub>2</sub> (95/5). The spatial resolution for a minimum

ionizing particle is 4 mm in X and 5 - 6 mm in Z.

### 3. 2 Preparation, Data Taking, and Calibration Procedures

#### 3.2.1 Final Preparation of Modules

The final preparation of modules for cosmic ray data acquisition involved tasks both on and off the test stand. In order to save set up time on the test stand, modules were checked for light tightness, chambers were gas purged, hadron calorimeter phototube voltages were set using external radioactive sources, and EM calorimeter phototube voltages were roughly set in a preparation area. As is described below operating the EM phototubes at roughly their nominal voltage values 1-2 days before the module was placed on the test stand kept small any gain drifts caused by "settling" of the tube high voltage.

The EM calorimeter phototube high voltages were set to their final values when the module was installed on the test stand, just before cosmic ray data were taken. The gain of each tube was adjusted to nominally produce 2 pC per GeV of energy deposited in the calorimeter. High voltage setting was performed by measuring the current produced by a Cs-137 calibration source inserted into the calorimeter near shower maximum and adjusting the voltage to give a predetermined target current. A complete description of the method can be found in Ref. 10. Voltages for individual EM and hadron tubes were controlled by motor driven potentiometers located in the high voltage distribution box, and could be read out through a CAMAC interface module to an accuracy of 0.5 V. The absolute scale of the voltage readout was calibrated on each distribution box. Once a tube voltage was set, no further adjustments to the potentiometer were made as the module moved from the test stand to the test beam, to the experimental collision hall. The calibrated readout allowed the bulk high voltage to be correctly set for the module in each location. This aided greatly in maintaining constancy of the calorimeter response when the module was transported.

#### 3.2.2 Data Acquisition Procedure

Before beginning the extended period of dedicated cosmic ray data acquisition several Cs-137 source calibration runs were taken for both the EM and hadron calorimeters. The voltage across the feedback resistor in the front end photomultiplier

charge integrator is proportional to the current supplied by the phototube and is available to the scanning ADC for digitization. A source calibration run consists of moving the Cs-137 calibration source through a brass tube installed in the calorimeter at shower maximum and mapping the response of each tube as a function of position of the source. The data are fit to obtain the peak response of each tube which is maintained as the primary calibration figure. Source runs were again taken at the end of cosmic ray data taking. The calibration runs were used only as a monitor of the response of the EM phototubes and were not used to make any corrections on the cosmic ray data.

Comparisons have been made of the source response difference at the beginning and end of cosmic ray data taking for the EM phototubes. These indicate that the response is quite stable over the typical 4 - 5 day period during which cosmic ray data are taken. Figure 5 shows the percent difference between start and end source response for each tube from 26 modules. The average difference is -0.21 % and indicates that the tubes settle to a slightly higher gain during the course of cosmic ray data taking. This drift is presumably due to the fact that the final voltage adjustments on the tubes are made just prior to taking the set of source calibration runs at the beginning of cosmic ray data taking. Thus, the gain may not have settled completely at this time. Most tubes drift less than 1 % during data acquisition. The drift has the effect of smearing out the minimum ionizing peak slightly. Since each mesh point in a tower is affected in an identical way and the response at each mesh point is normalized to the central response (see section 3.3), this small drift has a negligible effect on the cosmic ray response map.

Before beginning the several day period of dedicated cosmic ray data taking, a pedestal run was taken to provide both a final check that the complete system was operating correctly and a set of initial pedestals for subtraction from the signals. During the extended data run, pedestals were updated once an hour under computer automation by taking a sample of 200 pedestal events triggered by an external pulse generator. The pedestals generated in this way were used for online analysis only. As is discussed below the offline analysis recalculated pedestals every 250 events using data from non-trigger towers.

During cosmic ray running event data were written to disk. A run consisted of 40,000 cosmic ray event triggers and took

approximately 10 hours. Data taking proceeded essentially automatically with the computer handling generation of new runs and with operator intervention only to copy events from disk to magnetic tape and to check that the entire system was still operating correctly. The disk cleanup was part of an operator submitted batch job that copied events to magnetic tape, deleted the file from the disk to provide space for the next run, and ran the first pass offline analysis on the copied events. Doing the offline analysis immediately at the completion of the run had the advantage of giving us quick feedback on the data quality in a more detailed fashion than was available online.

Data quality was monitored online by a variety of histograms that were accumulated through the extended run period. Quantities histogrammed included pedestal subtracted pulse heights for each EM and hadron tube, the several largest pulse heights from the strips and wires in the strip chamber, hit profiles of strips and wires in the strip chamber, number of wires and strips hit per event, hit patterns for the muon drift chamber TDC's and ADC's, relative trigger rates of each tower for cosmic rays, and words recorded per event. These histograms were checked at 10 hour intervals as part of the operator service job.

### 3.2.3 Front End Electronics Calibration

All front end electronics servicing the phototube, strip chamber, and muon drift chamber systems proved to be quite stable over a period of many months. Since the phototube pulse heights were the critical measurements made at the test stand, the gains of the charge integrators and the current readout channels were routinely recalibrated and updated in the offline analysis approximately every two weeks. Calibration was performed in a front end electronics test crate with the ADC scanner interfaced to an IBM personal computer. Known charges were injected to the amplifier by charging a 472 pF capacitor with pulses from a programmable BNC 9010 pulse generator. The observed pulse heights from the charge integrator were fit to a straight line to obtain the amplifier gain. The current channel was calibrated by injecting current from a Keithley 261 Picoampere Source. Figures 6(a) and 6(b) show, respectively, representative plots of channel gains as a function of time for the charge and current channels. The current channel gains shown are from two prototype amplifier boards. The final version of the electronics has a nominal current channel gain of 11 pA/ADC count and boards of this type

were used during the last three months of operation of the test stand. The data of Fig. 6(b) are shown since these cards were in service for a longer period and have more calibration data available. The stability of the newer electronics has been found to be equal to that of the prototypes. The obvious feature of the charge calibration plots is the similarity in the gain fluctuations from channel to channel. This suggests that the front end electronics is more stable than the calibration system. The absolute gain of the charge channels is, thus, uncertain to a level of as much as 2 % while the absolute gain of the current channels is known to approximately 0.5 % which is quoted accuracy of the current source. Ignoring systematic variations and considering only the relative stability, the figures indicate that the charge amplifiers' gains are constant to a level of 0.76 % while the current gains are stable to 0.10 %.

The electronics servicing the muon and strip chambers did not need periodic calibration since the gains were stable enough for the accuracy required for tracking. The muon TDC and ADC system was only calibrated when CAMAC modules were replaced. The gains of the strip and wire amplifiers for the strip chamber were preset to within a few percent via adjustable capacitors, to 0.25 fC/ADC count and 1.0 fC/ADC count, respectively, and no calibration was required when replacing the electronics boards.

### 3.3 Data Analysis

A total of 50 modules were tested at the cosmic ray test stand. Typically about 200,000 events were used for making response map for each module. With a total of 200,000 events and a required statistical precision of 1 - 2 %, it was possible to subdivide the ten towers into a 650 element grid. The mesh size was typically 4.4 cm by 3.3 cm for towers 0 - 4 and 4.4 cm by 4.0 cm for towers 5 - 9 on the plane at the strip chamber depth.

The response was obtained from the sum of 2 tube outputs for each mesh element. The measurement of response of minimum ionizing particles is sensitive to the pedestal variation for a long run time such as was typical during normal data acquisition. Correction for the time variation of pedestals was made in the offline analysis.

#### 3.3.1 Response Maps

The definition of local coordinates in a tower is shown in Fig. 7, where  $Z$  (also  $\theta$ ) is the coordinate along the beam direction and  $X$  (also  $\phi$ ) is the one around the beam axis in the configuration of proton-antiproton collisions. The boundaries of  $X$  and  $Z$  in a tower are  $-12 \text{ cm} < Z < 12 \text{ cm}$  and  $-23 \text{ cm} < X < 23 \text{ cm}$ , respectively. The mesh elements on the plane of the strip chamber are defined by dividing the strips into 65 groups in  $Z$  and wires into 10 groups in  $X$ .

As stated previously, 200,000 cosmic ray events per module gives a statistical precision of 1 - 2 % for each mesh element. The response data is normalized to the response in the central area of a tower,  $|X| < 8 \text{ cm}$  and  $|Z| < 5 \text{ cm}$  in this case.

Although the pulse height distribution of muons is expressed by a convolution of 31 Landau distributions, a fit to a Gaussian function was adequate to estimate the peak value. For incident particles crossing the tower boundaries, which are mostly rejected in triggering, the response is obtained by summing the pulse heights in two adjacent towers.

### 3.3.2 Parametrization

The calorimeter response along  $X$  was expected to be symmetric from the structure of EM calorimeter. It is observed that the light attenuation curve viewed by a single phototube is not a simple exponential function. The main reasons for this seem to be due to the wave length dependence of the attenuation and light reflection at both edges of scintillators contacting with the waveshifters. As for the edge, the light collection is different from that in the central region due to the presence of a gap between neighboring waveshifters as mentioned in section 3.1.1.

In fitting the response in  $X$  to a function, the following parametrization is chosen:

$$P_0 + P_1 = A \cosh(X / w) ,$$

where  $P_0$ ,  $P_1$  are the phototube pulse heights, and  $A$  and  $w$  are parameters which are functions of  $Z$ . The following parametrization is also made:

$$P_0 / P_1 = B \exp(- 2 X / L) ,$$

where B and L are parameters which are functions of Z, and L corresponds to the conventional attenuation length.

### 3.3.3 Time Variation of Pedestals

Data taking runs continued for about 4 days in order to accumulate 200,000 events per module. A significant time variation of pedestals against the muon pulse height was observed during the run. The time variation of pedestals in a worst case amounts to 7 - 8 % of the muon peak value. The correction was made in the offline analysis by using the fact that all tubes were read out for each cosmic ray event, not just those in the trigger road. This allowed an event-by-event pedestal to be accumulated using all towers not associated with the trigger. In this procedure, the average pedestal value for each tube was calculated every 250 triggers which correspond to a running time of 2 - 3 minutes.

## 3. 4 Results

### 3.4.1 Muon Pulse Height Distribution

A typical pulse height distribution for cosmic ray muons viewed by a single phototube is shown in Fig. 8(a) and (b). Figure 8(c) is the distribution viewed by two phototubes, i.e.  $(P_0+P_1)/2$ . As seen in Figs. 8(a), (b) and Fig. 8(c) the distributions have an rms width of 20 - 21 % and 16 - 17 %, respectively.

The main contributions to the width of the peak are: (a) statistical fluctuation in sampling photoelectrons, (b) Landau fluctuation in energy deposited in each scintillator, (c) variation in path length due to different incident angles of the cosmic ray muons, (d) position dependence of the light attenuation.

Figure 9 shows the number of photoelectrons per GeV for each tube of a module obtained using LED measurements and the nominal gain calibration figure of 2 pC per GeV per phototube. The average number of photoelectrons per GeV is estimated to be 115 from LED measurements for several modules, and was confirmed by the electron beam test. Thus the fluctuation in photoelectron statistics  $1 / (N_{pe})^{1/2}$  is 17.0 % for an EM shower energy of 0.3 GeV, corresponding to the calorimeter response for the muon. The

Landau fluctuation in multi-layer traversal was calculated by a Monte Carlo simulation. The value ranges from 4.5 % to 9.7 % depending on the tower number. These values include the effect of (c) which varies from 1 to 6 % with increasing tower number. The value 4.5 % in tower 0 is consistent with the value calculated from a simplified formula given, for example, by Amaldi [11] which typically gives 4.5 %. The variation in the response due to position dependence is also estimated by a Monte Carlo simulation to be 11.5 % for a single tube, 2 % for  $(P0+P1)/2$ .

Thus the total contribution is expected to be about 21 - 23 % for the case of single tube and 13 - 16 % for the case of the two tubes. These estimates are consistent with the observations.

The average muon peak value for all towers in the EM calorimeter was  $623 \text{ fC} \pm 37 \text{ fC}$ . Since the calorimeter gain was set to be 2 pC/GeV/phototube, the calorimeter response for a minimum ionizing particle was estimated to be 0.31 GeV. The average and rms values of the peak pulse height for each tower over 44 modules are tabulated in Table 1.

We notice here that the peak value of cosmic ray muons is different from that of punch-through particles (mainly non-interacting pions) of 50 GeV in the beam test as shown in Fig. 10. The data for all the towers 0 - 8 of 6 modules are plotted in the figure. No significant tower dependence is found. It is seen that the test beam data are higher than the cosmic ray data by, on the average, as much as 10 %. This seems to be due to the fact that when the energy of muon and punch-through particles increases other processes than ionization, such as bremsstrahlung, pair production and so on, take place more frequently in the calorimeter and give a higher most probable peak value.

### 3.4.2 Similarity of The Response Map

Study of the similarity of the response maps tower-to-tower and module-to-module over all modules is essential for the cosmic ray test. A total of 41 modules with the data having more than 150,000 events were used for the study.

The similarity for module-to-module is defined in terms of the deviation from the average response value at each mesh point

over all the modules tested. The average response is shown in Fig. 11. The overall rms deviation obtained in this way is 1.5 %, where the data of tower 9 are excluded. The value still involves a statistical uncertainty.

We redefine the intrinsic systematic dissimilarity as follows:

$$D_{ij}^2 = 1/N [ \sum_m ( R_{mij} - R_{ij} )^2 - \sum_m dR(\text{stat})_{mij}^2 ],$$

where  $R_{mij}$  is the normalized response in mesh element (i,j) of module m,  $R_{ij}$  is the average response for all N modules in mesh element (i,j),  $dR(\text{stat})_{mij}$  is the statistical component of the deviation of response in mesh element (i,j) of module m.

The resulting mean value of D and its rms deviation over the whole area are 0.95 % and 0.47 %, respectively. Here no tower dependence on D's is observed. However there exists a dependence of D on the regions in a tower. Figures 12(a) - (d) show the distributions of D's in towers 0 - 8 for four different regions, i.e. the entire region, the central region ( $|X| < 17$  cm,  $|Z| < 10$  cm), the theta-edge region ( $|X| < 17$  cm,  $|Z| > 10$  cm) and the phi-edge region ( $|X| > 17$  cm,  $|Z| < 12$  cm), respectively. As is seen in Fig. 12(b) the dissimilarity obtained in the central region is 0.76 %. The average and rms values of dissimilarity for each tower were calculated using all of the 41 modules and are listed in Table 2(a) dividing into several regions.

Next, the X dependence of D is examined. The average dissimilarity along a fixed X is presented in Table 2(b). The average value increases as X increases. The value in the region of  $|X| > 17$  cm exceeds 1 % for towers 0 - 8.

### 3.4.3 Parameters w And L

The parameters w and L were obtained for 65 points in Z defined by strip groups, where each tower consists of 6 - 7 groups. A typical response map in x at the Z center in a tower is shown in Fig. 13(a), where the solid curve is fit to an expression  $\cosh(X/w)$  for the region  $|X| < 17$  cm. The distribution of the ratios of two tube outputs in X at the Z center is shown in Fig. 13(b), where the solid curve is fit to  $\exp(-2 X/L)$  again for the same region  $|X| < 17$  cm. The errors in w and L in the above fitting are 1 % and 5 %, respectively.

Figures 14(a) and (b) show the distribution of w's and L's

at the Z center of each tower over 46 modules. The average values of w and L are 55.0 cm and 99.3 cm, respectively. Here we examine the tower-to-tower and module-to-module deviations in w's and L's obtained at the tower centers. The result is listed in Table 3, and indicates that the deviations from tower-to-tower within a module for both quantities are significantly smaller than those for module-to-module. This may be a consequence of the quality control in production of the calorimeter modules.

The Z dependences of w's and L's for 46 modules are shown in Figs. 15(a) and (b) respectively, in which the data points are normalized by their average values at tower centers. As is seen in the figures, the mean value of L increases as the hit position becomes closer to the tower boundary, while that of w does not show clearly such a trend within the spread of about 9 % of the rms deviations. One of the reasons for the difference is considered to be due to the fact that the cosmic ray data involves incident particles with different impact angles, which causes a change in track lengths within a certain angular acceptance. The effect seems to be more sensitive to w than L because in the derivation of L, the ratio of two phototube outputs is involved, which tends to cancel the above effect.

In order to test this point, we chose a particular module with high statistics and required that the muon tracks pass through the same subdivision, divided into 12 per tower, in the upper and lower muon chambers. The result indicates that the value of w is reduced by 12.3 % while that of L is reduced by only 3.5 %. In this sense, the cosmic ray test with the present procedure is capable of providing a reliable value of L. The increase of L in approaching to the tower boundary is obviously due to an effect of the presence of a gap in the light collection at the tower boundary.

The dependence of L on Z for each tower can be expressed by using a polynomial:

$$L = L_0 (1 + C_1 Z + C_2 Z^2) ,$$

where  $L_0$  is the value of L at each tower center of each module. The resultant fits are shown in Fig. 16 as the solid curves. The average and deviation in these values for each tower using 46 modules are presented in Table 4.

Figure 17 shows the correlation plot between L and w using the

values at tower centers of tower 0-8 over 46 modules. We note here that a clear significant correlation can be seen by dividing the distribution into two groups. The difference in the two groups can be related to the different batch number in production of scintillator boards. The correlation in each group can be expressed as  $w=0.60 \cdot L$  and  $w=0.50 \cdot L$  respectively.

Finally we mention the magnitude of deviation of the response reflected from the deviation of  $w$ . The average value of  $w$  is 55.0 cm and the module-to-module deviation is 9.2 %. The deviation of the response  $R$  in terms of that of  $w$  is expressed as follows.

$$dR/R = (dw/w) (X/w) \tanh( X/w ) ,$$

where  $R = A \cosh( X/w )$ . At  $X = 15$  cm and 20 cm, for example, the values  $dR/R$  are 0.7 % and 1.2 %, respectively, which are consistent with the results of dissimilarity shown in Table 2(b).

#### 3.4.4 Long-term Stability

We have studied the long-term stability of the central EM calorimeter by comparing the cosmic ray test data for a particular module (No.17) taken at an interval of 7.5 months [12].

The following possibilities would cause the deterioration of the calorimeter response: (a) damage to fluors in the scintillator, (b) decrease in the transparency of the scintillator base, (c) deterioration of the light collection system which consists of the wavelength shifter and light guide, (d) change of the tube gain.

The pulse height was measured to estimate effects (a) to (d). The measurement of the attenuation length ( $L$ ) was useful for estimating (b).

Details can be found in Ref.12. The following conclusions are drawn:

- (1) The deterioration in muon pulse height is estimated to be  $2.0 \pm 0.6$  % per year.
- (2) The deterioration in the attenuation length ( $L$ ) is  $2.7 \pm 2.9$  cm per year.

#### 3.4.5 Comparison with Beam Test Results

For the mapping purpose in the beam test, 5 modules were scanned precisely with 50 GeV electrons [13]. The response at each point was measured with a statistical error of less than 0.5 %. The mesh size was chosen to be 1 cm by 1 cm, while the impact point separation and beam size were 4 cm and 2.5 cm in diameter, respectively [14].

The similarity for each mesh was examined in the same manner as that for the cosmic ray data. The overall rms deviation in dissimilarity is found to be 0.8 %. The deviation in the central area ( $|X| < 20$  cm and  $|Z| < 10$  cm) is 0.6 %. Typical response maps as a function of Z are shown in Fig. 18. Since the tower structure differs in its geometical characteristics for tower 0, towers 1-8 and tower 9, the Z response map is shown separately in Figs. 18(a), 18(b) and 18(c), respectively. The response maps from the cosmic ray muons for this particular module are also shown in the figure. Shown in Figs. 19(a), 19(b) and 19(c) are the response maps in X at the tower center in the same module and same towers above mentioned. The corresponding cosmic ray muon data are also shown in the figures.

The above figures indicate that mapping with cosmic ray muons does not produce accurate and useful maps of response for theta-boundaries and phi-edges. This mapping should be made by scanning with the electron beam. In fact, the precise mapping and uniformity correction have been made with an electron beam. [14]

The parametrization of the response map by w and L in X is made for electron data, which is to be compared with those from cosmic ray data. The mean values of w's and L's from electron data are 44.3 cm and 88.5 cm, respectively. The values are those obtained from the data in the range  $|X| < 19$  cm. The values are smaller than those from cosmic ray data by 18.0 % and 9.5 %, respectively. The fact is already mentioned and explained in Section 3.4.3. The rms deviations of w and L obtained from 5 modules are 10.3 % and 3.8 %, respectively. The correlation between w and L is also examined. A larger dispersion from module-to-module than for tower-to-tower is observed as in the cosmic ray data.

### 3.5 Discussion and Conclusion

Response mapping of the central EM calorimeter modules has been performed with cosmic ray muons. The correspondence of response maps obtained with electron test beam is also made. As described previously, there is a fairly good correspondence between cosmic ray and electron beam data.

In actual case, the correction function for response maps is provided from the fine scanning with an electron beam for 5 modules. The resultant correction function is a product of functions of hyperbolic cosine of  $X$  with a parameter  $w$ , exponential of polynomials of  $X$  and  $Z$ , and polynomial of  $Z$ . The correction function with average parameters turns out to be capable of obtaining reproducibility with an rms deviation of 1.1 % for each tower, except for the region of phi-edges ( $|X| > 20$  cm). Details of the treatment for the phi-edges can be found in Ref.14.

The most sensitive parameter in the correction function is  $w$  (or  $L$ ). In order to guarantee the reproducibility to be at the 1 % level, it is found that the values of  $w$  (or  $L$ ) must lie within 10 % of the average value derived from the electron beam test for 5 sampling modules. As can be seen in Fig. 14, the cosmic ray data for 46 modules shows that the distributions of  $w$  and  $L$  are not the normal ones and some towers have the values out of the range. In fact, 80 towers out of 460 towers tested are out of the required range in the value of  $L$  which is more reliable to count than that of  $w$  in case of cosmic ray data. In other words, a global correction function with the average parameters can guarantee the reproducibility to be at the 1 % level for a set of 380 towers. For the rest of the towers the parameter  $w$ , in particular, needs to be modified individually from the average value. That is, for towers having  $L$  value out of the required range, the actual value of  $w$  in the correction function is modified from the average by multiplying a factor composed of the ratio  $L/L(\text{average})$  and the correlation coefficient between  $w$  and  $L$ .

In this sense, the cosmic ray data plays an important role in providing the individual parameter for every tower of the whole modules. Either the average parameters from solely the electron beam data or the combined parameters from both the electron beam and cosmic ray data can be implemented in the data base depending on the required precision.

Finally, the performance of the EM calorimeter in the cosmic ray test is summarized as follows:

- (1) The similarity of response maps is measured to be within 1 % for the central region ( $|X| < 17$  cm,  $|Z| < 10$  cm), and 1.2 % on average for the outer region ( $|X| > 17$  cm,  $|Z| > 10$  cm).

- (2) The parametrization of the correction function for the response maps in X and Z is performed.
- (3) The correction parameters for the mapping from the cosmic ray test is combined with those from electron beam test in order to achieve an even reproducibility for all modules. The resultant correction function is capable of obtaining reproducibility with an rms deviation of 1.1 %, except for the region of phi-edges.
- (4) The long-term stability of the calorimeter response is tested with cosmic rays. Possible deterioration is estimated to be  $2.0 \pm 0.6$  % per year.

## 4. HADRON CALORIMETER

The procedures for the data acquisition were the same as for the EM calorimeter described previously and carried out simultaneously. Details of the present analysis can be found in Ref. 15.

### 4. 1 Calorimeter Description

A detailed description of the hadron calorimeter and its performances can be found in Refs.[1(a)] and [1(c)]. The hadron calorimeter is a stack of alternating scintillators[16] and iron plates, each 1 cm and 2.54 cm thick respectively. It consists of 48 modules and each module has 8 projective towers numbered 0 to 7, starting at 90° in  $\theta$ . Towers 0 to 5 have 32 scintillator layers, while towers 6 and 7 have 19 and 10 scintillator planes only.

Scintillation light is collected by two wavelength shifter strips[17] on the two long scintillator sides. The wavelength shifter emitted light is transported to the phototube by UVA PMMA strips of the same dimensions ( 0.5x1.0 cm<sup>2</sup> ), as shown in Fig. 20. On each side of a calorimeter tower all the 32 plexiglass strips are folded together and coupled to a 2" phototube, EMI 9954.

### 4.2 Preparation and Monitoring of Phototube High Voltage Setting

The high voltage of the hadron calorimeter phototubes was determined in the following way. First of all, the light output from each scintillator plane was made equal, by irradiating each plane with a Cs-137 source and by inserting paper filters between each wavelength shifter-UVA PMMA strip transition. This adjustment was done in the production line before mounting the wedge module on the cosmic ray test stand.

Let us define  $\eta(i,j)$  the light collection efficiency of the  $i$ -th tower of the  $j$ -th wedge . The signal charge  $q(i,j)$  is related to the phototube gain  $g(i,j)$  and to the light yield  $S(i)$  generated in a tower by the relation:

$$q(i,j)=S(i)\cdot\eta(i,j)\cdot g(i,j).$$

$q(i,j)$  was made  $j$ -independent by adjusting the gain. Since the light-guides are independently equalized there may be small  $g(i,j)$  differences even between two phototubes viewing the same tower.

This adjustment was performed by running a Cs-137 gamma-source

along a fixed path on both longitudinal sides of each tower and by changing the high voltage until the same current was reached for all phototubes. A reference gain was chosen for all phototubes such that a 50 GeV/c pion would give a charge of 100 pC.

To monitor the phototube gain at any time two independent ways are provided: a Sr-90 beta source can be located in a reproducible position on the light guide in front of the photocathode; a Cs-137 source can be driven through different towers at a fixed calorimeter depth.

## 4. 3 Results

### 4.3.1 Muon Pulse Height Distribution

Figure 21 shows a typical muon pulse height distribution obtained in the cosmic ray stand, integrated over the full polar and azimuthal acceptance of a tower. In order to ensure that muon trajectory is fully contained, we require the pulse height in each adjacent tower to be less than 1.5 time the width of the pedestal fluctuation. We fit the muon pulse height distribution with a Gaussian and find the peak value to be close to the most probable value of the distribution. The phototube gain has been normalized to the reference gain. The ADC gain has been measured separately.

Figure 22 shows the distribution of the muon peak values for a sample of 12 wedge modules. Measured values are corrected for different tower thicknesses. Table 5 shows the average and standard deviation of the muon peaks distribution for all towers 0 to 3. We conclude that the calorimeter equalization and phototube high voltage setting are established with an accuracy better than 6%. The last column in Table 5 shows the test-beam result[18] which is in a good agreement with cosmic ray data.

We compared the cosmic ray muon data with the 50 GeV pion data[18] for a sample of 5 wedge modules. Table 6 shows the averages and the widths of the pion peak distributions for towers 0 to 3. The 50 GeV pion and cosmic ray muon responses are found to be proportional within a few %. The last column in Table 6 expresses the muon signal in GeV.

### 4.3.2 Number of Photoelectrons

Using the three planes of tracking chambers, we selected muons passing through the tower center within  $\pm 2$  cm. The width of the pulse height distribution is contributed by statistical fluctuations of the number of photoelectrons ( $N_{pe}$ ) and by fluctuations of the signal itself. To get rid of this last effect we derived the number of photoelectrons from the widths of the  $\log(R/L)$  distributions, as well as from the width of the  $(R+L)$  and

(R-L) distributions. If we assume the response of two calorimeter sides to be equal, the number of photoelectrons is related to those distributions in the following way:

$$N_{pe}(1) = 2 / \sigma^2 (\log(R/L))$$

$$N_{pe}(2) = 2 \mu^2 ((L+R)/2) / \sigma^2 (R-L),$$

where  $\sigma$  and  $\mu$  indicate the rms and the mean of the distribution. Table 7 shows the results for towers 0 to 4.

From Monte Carlo simulation we expect  $N_{pe}(1) < N_{pe}(2)$  and the true photoelectron number to be close to the average of  $N_{pe}(1)$  and  $N_{pe}(2)$ . Table 7 confirms the systematic expected difference between the two methods of calculation.

Since the equivalent mean energy released from a muon in tower 0 is  $1.8 \pm 0.3$  GeV ( see Table 6), the produced number of photoelectrons/GeV is  $11 \pm 3$  when observed by a single phototube. The value should be considered as a lower limit because the long term period of data taking ( about 11 hours) caused an increase of the rms.

#### 4.3.3 Attenuation Length of Scintillator

The light attenuation length in the calorimeter was measured by selecting muons passing at a distance of  $\pm 11.5$  cm from the calorimeter Z-axis, in the region 4 cm wide along the same axis, on the plane separating hadron and EM sectors.

For those tracks the attenuation length L is connected to the ratio of the phototube pulse heights as  $L = 23 / |\log(R/L)|$ , where R and L are the mean of the pulse height distribution as seen by each phototube. Table 8 gives the attenuation length calculated for towers 0 to 3. The average attenuation length is  $120 \text{ cm} \pm 10 \text{ cm}$ .

#### 4.3.4 Uniformity Check

The calorimeter response uniformity as a function of the muon position was also studied.

Using the track chamber information, a tower is divided into three equal regions along Z and into three different X regions, namely  $-30 \text{ cm} \leq X \leq -20 \text{ cm}$ ,  $-5 \text{ cm} \leq X \leq 5 \text{ cm}$  and  $20 \text{ cm} \leq X \leq 30 \text{ cm}$ . The nine mesh elements are defined on the middle Y plane of the calorimeter.

Figure 23 shows a typical distribution of the average pulse heights of single phototubes for cosmic ray muons entering different Z regions with X

between -5 cm and +5 cm. Figure 24 shows the distribution of the average sum of the responses of phototubes for all X and Z regions. From the full width at half maximum of the distribution we estimate a response uniformity better than 2.8 %.

#### 4. 4 Conclusion

We measured some properties of the CDF hadron calorimeter by using cosmic ray muons.

Response uniformity is found to be better than 3 %. The photoelectron yield in a tower is measured to be about 20 photoelectrons/GeV by comparing with test beam results. The average attenuation length of scintillator is obtained to be  $120 \text{ cm} \pm 10 \text{ cm}$ .

The test provided prompt control of the production quality.

#### 5. SUMMARY

The mapping measurements for the EM calorimeter are performed with cosmic ray muons. The correspondence between cosmic ray and beam test results indicates that the mapping with cosmic ray muons is quite useful for a large number of calorimeter modules, except for the edge regions of the module.

The cosmic ray test is also capable of deducing some of the basic characteristics of hadron calorimeter to be consistent with those from the beam test.

#### ACKNOWLEDGEMENT

This work was greatly assisted by the continued efforts of the Fermilab crews conducted by R. Krull and by R. Peto of Argonne National Laboratory in Industrial Building IV at Fermilab. We would like to acknowledge the valuable advice and assistance of D. Bauer, J. Cooper, and H.H. Williams in connection with the development of the source calibration system. One of us (A.D.V.) would like to thank S. Bertolucci, B. Esposito, A. Garfinkel and A. Sansoni for useful discussions and P. Giromini for careful reading of the manuscript. The work was supported by the U.S. Department of Energy Contract DE-AC02-76CH0-3000.

#### REFERENCES

\*) Now at the Texas A & M University.

\*\* )Now at INFN, Pisa.

1. a) D. Ayres et al., Design Report for CDF, Fermilab CDF Note 111 (1981), (updated, unpublished).  
b) L. Balka et al., The CDF Central Electromagnetic Calorimeter, submitted to Nuclear Instruments and Methods.  
c) S. Bertolucci et al., The CDF Central and End Wall Hadron Calorimeter, submitted to Nuclear Instruments and Methods.
2. Collaboration at this stage by V. Barnes, S. Bertolucci, M. Curatolo, R. Diebold, Y. Fukui, P. Giromini, H. Jensen, E. May, A. Sansoni and D. Underwood is appreciated.
3. P.J. Green et al., Phys. Rev. D20 (1979) 1598.
4. T. Kamon et al., Fermilab CDF Note 279 (1985); G. Ascoli et al, CDF Central Muon Detector, submitted to Nuclear Instruments and Methods.
5. N. Solomey and A.B. Wicklund, Fermilab CDF Note 247 (1984).
6. G. Drake et al., Fermilab CDF Note 358 (1985); G. Drake et al., Fermilab CDF Note 357 (1985); G. Drake et al., Front End Electronics : The RABBIT System, submitted to Nuclear Instruments and Methods.
7. J.L. Schlereth and E.N. May, MIDAS User's Guide, DAN-4 (1983).
8. The scintillator SCSN-38 and wavelength shifter Y-7, manufactured by Kyowa Gas Chemical Ind. Co. Ltd., Nihonbashi, Chio-ku, Tokyo, Japan; See also T. Kamon et al., Nucl. Instr. and Meth. 213 (1983) 261.
9. T. Devlin et al., Phototube Testing for CDF, submitted to Nuclear Instruments and Methods.
10. R.G. Wagner et al., Fermilab CDF Note 374 (1986).
11. U. Amaldi, Physica Scripta, 23 (1981) 409.
12. T. Kamon et al., Fermilab CDF Note 299 (1985).
13. J.W. Cooper et al., Private communications.
14. K. Yasuoka et al., Fermilab CDF Note 399 (1986); K. Yasuoka et al., Response Maps of the CDF Central Electromagnetic Calorimeter with

Electrons, submitted to Nuclear Instruments and Methods.

15. A. Di Virgilio, Fermilab CDF Note 457 (1986).
16. PMMA doped with 8 % Naphtalene, 1 % Butyl-PBD and 0.01 % POPOP, manufactured by Polivar, Pomezia, Italy.
17. PMMA doped with 30 mg/l of laser dye 481, manufactured by Polivar, Pomezia, Italy.
18. S. Bertolucci et al., Fermilab CDF Note 349 (1985).

#### TABLE CAPTIONS

1. Average and widths of cosmic ray muon peaks in the EM calorimeter.
2. a) Deviations in dissimilarity.  
b) Deviations in dissimilarity along X.
3. Average values and deviations of w and L.
4. Parameters in Z dependence of L.
5. Averages and widths of cosmic ray muon peaks (sample of 12 hadron calorimeter modules, towers 0 to 3). Last column shows average muon peaks measured with the test-beam (sample of 50 hadron calorimeter modules)
6. Average cosmic ray muon and 50 GeV pion peaks. Last column gives the averages of the ratios between cosmic ray muon and pion peaks.
7. Total number of photoelectrons as measured from L/R and from (R-L) distributions, and their average.
8. Estimated scintillator attenuation length on the plane separating the EM and hadron sectors.

#### FIGURE CAPTIONS

1. Schematics of the setup of the cosmic ray test stand.

2. Observed relative trigger rate for each tower. The total trigger rate is 1.8 Hz. The histogram shows the result of a Monte Carlo simulation.
3. Block diagram of the trigger electronics.
4. Block diagram of data acquisition control logic.
5. Difference between the average Cs-137 source calibration current at the beginning of cosmic ray data taking and at the end. The average is histogrammed for each tube individually in 26 different modules. The mean difference is -0.21 % and the standard deviation of the distribution is 0.62 %.
6. (a) Calibrated charge integrator gains as a function of date of calibration for three channels on three different boards. The data between June 1984 and December 1984 have been rescaled by a factor of 0.979 to correct for a change in the voltage calibration of the BNC 9010 pulse generator. The boards were prototype versions of the final front end electronics. The nominal gain of the charge channels was unchanged between the prototype and final versions.  
  
(b) Calibrated current amplifier gains as a function of date of calibration for two channels on two different prototype front end electronics boards. The final electronics design used a nominal gain of 11 pA/ADC count and had a stability similar to that implied by the data in this figure.
7. (a) Global coordinates in X and Z at the cosmic ray stand.  
  
(b) Local coordinates in X and Z in a tower. The typical size of a scintillator plate on the strip chamber is also shown in the figure.
8. (a) Typical pulse height distribution of cosmic ray muons viewed by a left tube in an EM calorimeter tower.  
  
(b) Typical pulse height distribution of cosmic ray muons viewed by a right tube in an EM calorimeter tower.  
  
(c) Typical pulse height distribution of cosmic ray muons viewed by two tubes in an EM calorimeter tower.

9. Number of photoelectrons per GeV for each phototube in a module from LED measurements.
10. Scatter plot of pulse heights of cosmic ray muons and 50 GeV punch-through particles.
11. Average response along Z for each fixed X over 41 modules.
  - (a)  $X = 15.3$  cm and (b)  $X = 2.2$  cm.
12. Dissimilarity distributions in towers 0-8, for four different regions.
13. (a) Typical response map in X at the Z center in a tower and fit to  $\cosh(X/w)$ .
  - (b) The distribution of the ratios of two tube outputs in X at the Z center in a tower and fit to  $\exp(-2 X/L)$ .
14. Distributions of w's and L's measured at tower centers.
15. Dependences of w and L on Z, where the values w and L are normalized by the average value over tower centers for each module.
16. Polynomial fit of Z dependence of L for each tower using 46 modules. The data are averaged  $L/L(\text{mean})$  over 46 modules.
17. Correlation plot of L and w using the values at the tower centers of towers 0 - 9 over 46 modules.
18. Typical Z-response maps with cosmic ray muons and electrons.
19. Typical phi-response maps with cosmic ray muons and electrons.
20. Light collection scheme of the hadron calorimeter.
21. Typical pulse height distribution of cosmic ray muons as seen by one phototube in a hadron calorimeter tower.
22. Distribution of muon peak pulse heights in the hadron calorimeter.
23. Distribution of muon peaks seen by each phototube at  $X=0$  for different Z values.

24. Distribution of muon peaks in a tower for all nine X,Z regions defined in the text.

Table 1

Tower	0	1	2	3	4	5
Average	595.31	599.20	616.02	603.71	602.81	609.99
Width	26.15	24.29	25.56	28.64	31.97	27.78
Tower	6	7	8	9		
Average	655.29	651.02	657.21	624.79		
Width	28.89	26.79	27.33	28.65	( unit: fC )	

Table 2(a)

Tower	All Area	Central Area	Theta-edge	Phi-edge	(*)
0	0.84 +/- 0.39	0.71 +/- 0.18	0.60 +/- 0.31	1.46 +/- 0.20	0.93
1	0.98 +/- 0.40	0.80 +/- 0.25	0.98 +/- 0.30	1.46 +/- 0.42	0.82
2	0.79 +/- 0.37	0.64 +/- 0.24	0.71 +/- 0.33	1.30 +/- 0.25	0.78
3	0.86 +/- 0.36	0.68 +/- 0.26	1.04 +/- 0.30	1.20 +/- 0.31	0.69
4	1.13 +/- 0.42	0.96 +/- 0.26	1.15 +/- 0.48	1.54 +/- 0.38	0.72
5	1.13 +/- 0.35	1.00 +/- 0.24	1.02 +/- 0.32	1.55 +/- 0.27	0.89
6	1.00 +/- 0.68	0.62 +/- 0.27	0.99 +/- 0.41	1.78 +/- 0.83	0.69
7	0.91 +/- 0.48	0.71 +/- 0.22	0.73 +/- 0.36	1.54 +/- 0.51	0.66
8	0.94 +/- 0.61	0.71 +/- 0.28	0.76 +/- 0.36	1.76 +/- 0.77	0.88
9	2.14 +/- 0.77	1.20 +/- 0.42	2.13 +/- 0.69	2.76 +/- 0.62	0.80
0-8	0.95 +/- 0.47	0.76 +/- 0.28	0.87 +/- 0.46	1.48 +/- 0.44	0.79
	( Average=1.20 +/- 0.55 )				

(\*) Dissimilarity from electron data for the whole area. For tower 9, the data for  $Z > 10$  cm are removed in estimating dissimilarity.

Table 2(b)

Median X (cm)	Wire Group Number	Dissimilarity (%)		
		Cosmic Ray Data		Beam Test
		Towers 0-8	Tower 9	Towers 0-9
0.0	5, 6	0.39 +/- 0.60	1.86 +/- 0.52	0.38 %
6.5	4, 7	0.66 +/- 0.32	1.79 +/- 0.75	-
10.9	3, 8	0.77 +/- 0.32	2.16 +/- 0.90	-
15.3	2, 9	0.93 +/- 0.27	2.18 +/- 0.55	-
19.6	1,10	1.48 +/- 0.44	2.76 +/- 0.62	1.77 %

Table 3

	Average (cm)	Tower-to-tower deviation (%)	Module-to-module deviation (%)
w	55.0	5.6	9.2
L	99.3	3.3	9.0

(1) The errors for w and L are typically 6 % and 2 %.

Table 4

Tower	$L_0$ (cm)	$C_1$ ( $\times 10^{**}-3$ )	$C_2$ ( $\times 10^{**}-3$ )
0	100.9 +/- 8.1	7.18 +/- 5.76	1.44 +/- 0.71
1	101.2 +/- 8.7	0.19 +/- 4.84	1.19 +/- 0.37
2	97.9 +/- 8.5	0.42 +/- 3.86	0.94 +/- 0.38
3	98.0 +/- 9.3	3.74 +/- 3.52	1.25 +/- 0.43
4	98.2 +/- 8.9	1.79 +/- 3.39	1.15 +/- 0.48
5	96.7 +/- 8.9	4.17 +/- 6.23	1.32 +/- 0.53
6	96.7 +/- 8.7	1.58 +/- 4.25	1.11 +/- 0.68
7	98.2 +/- 8.8	-0.03 +/- 4.12	1.20 +/- 0.53
8	99.9 +/- 7.9	0.90 +/- 3.81	1.26 +/- 0.63
9	85.9 +/- 6.3	-3.24 +/- 4.09	2.17 +/- 0.79

Table 5

Tower	peak (pC)	HWHM (pC)	HWHM(%)	peak (pC)(test-beam)[18]
0	4.26	0.22	5.2	4.3
1	4.29	0.30	7.1	4.4
2	4.51	0.24	5.4	4.5
3	4.90	0.27	5.4	4.9

Table 6

Tower	pion (pC)	width(%)	muon (pC)	width(%)	50GeVxmuon/pion
0	115.2	6.7	4.28	3.5	1.85
1	118.9	3.1	4.30	3.7	1.81
2	121.1	2.8	4.53	2.6	1.86
3	122.6	7.0	4.77	4.4	1.99

---

Table 7

Tower	$N_{pe}(1)$	$N_{pe}(2)$	Average
0	16.1 +/-0.5	20 +/- 1	18
1	18.7	21	19.8
2	17.3	22	19.6
3	20.3	28	24.2
4	21.2	28	24.6

Table 8

<u>Tower</u>	<u>L (cm)</u>
0	119
1	107
2	123
3	133

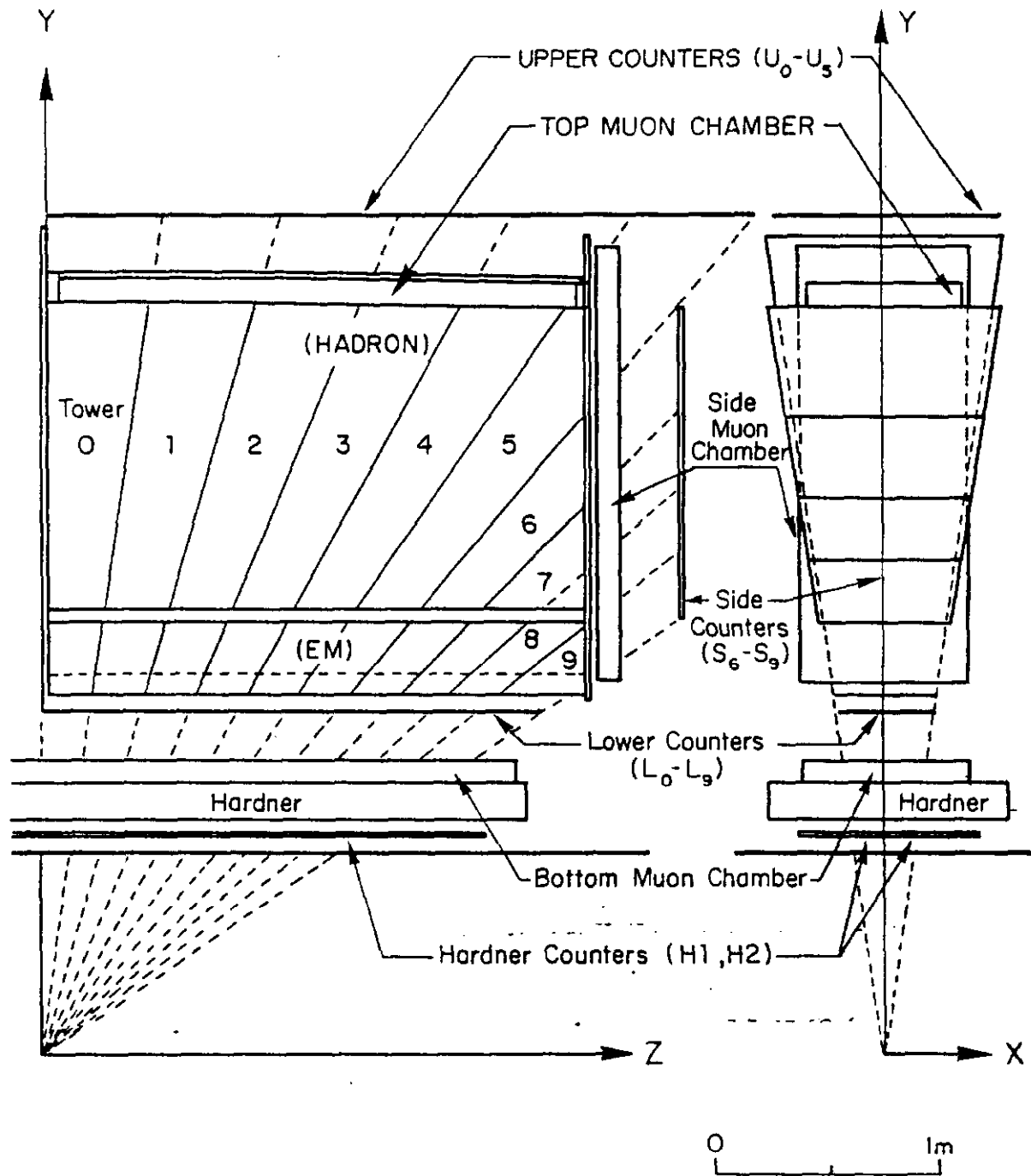


Fig. 1

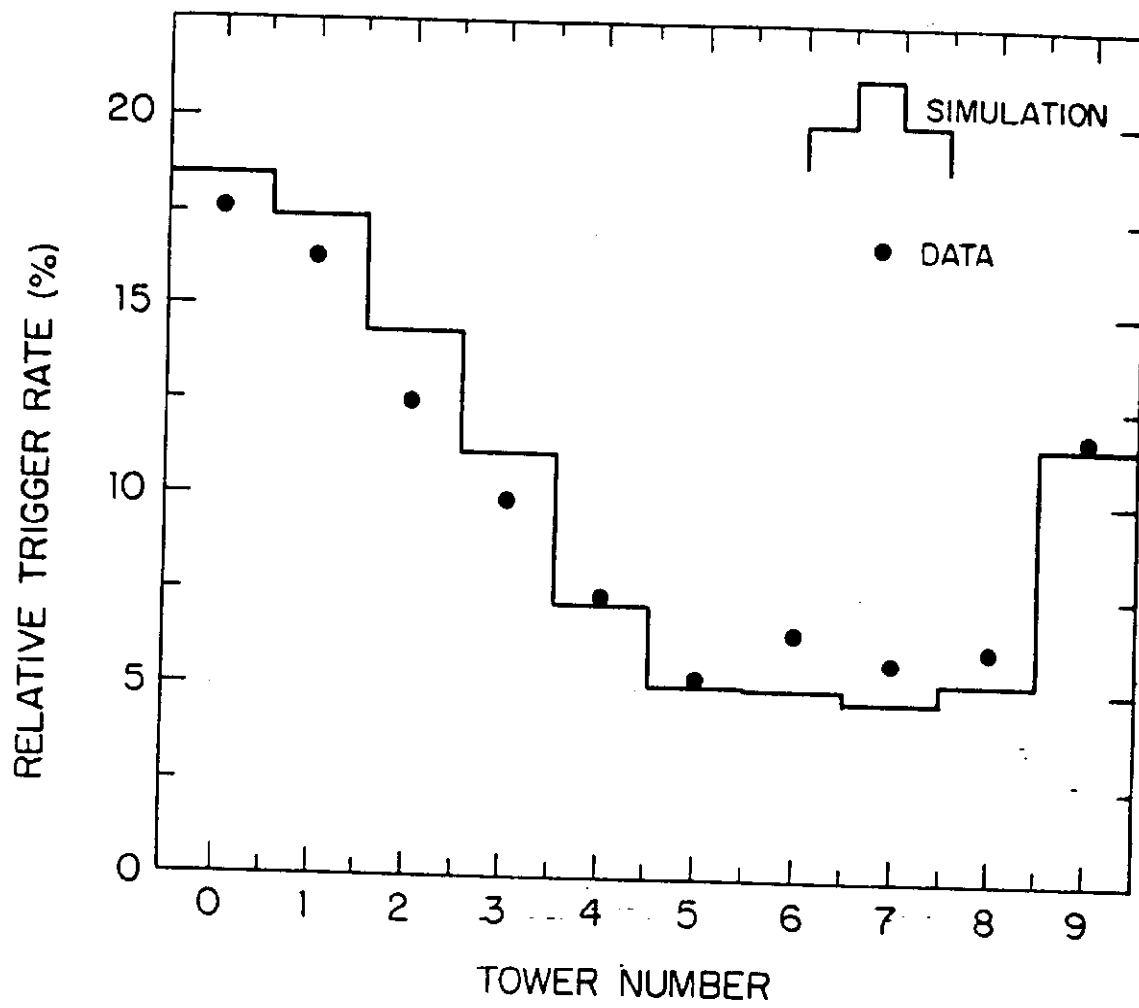


Fig. 2

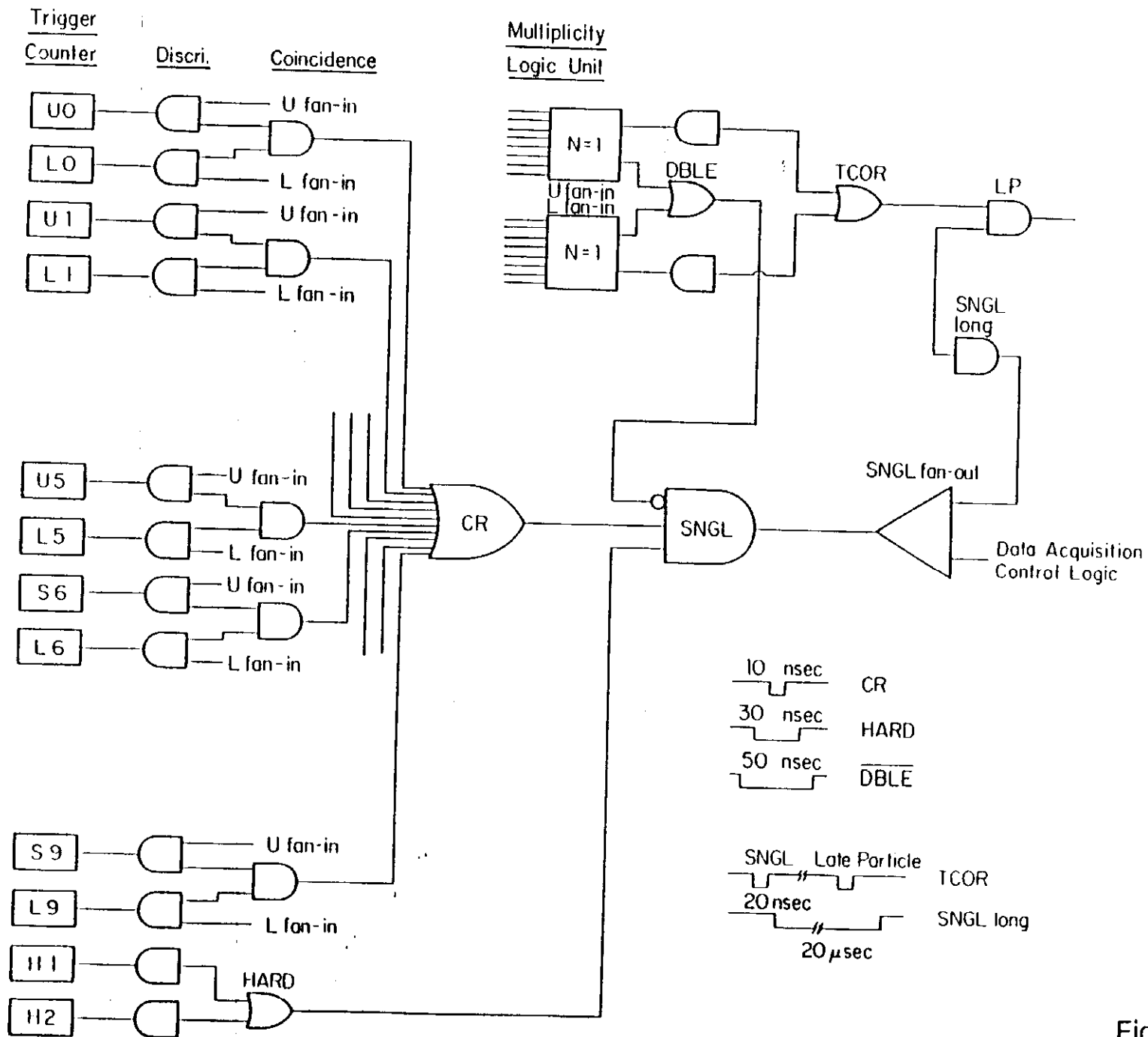


Fig. 3

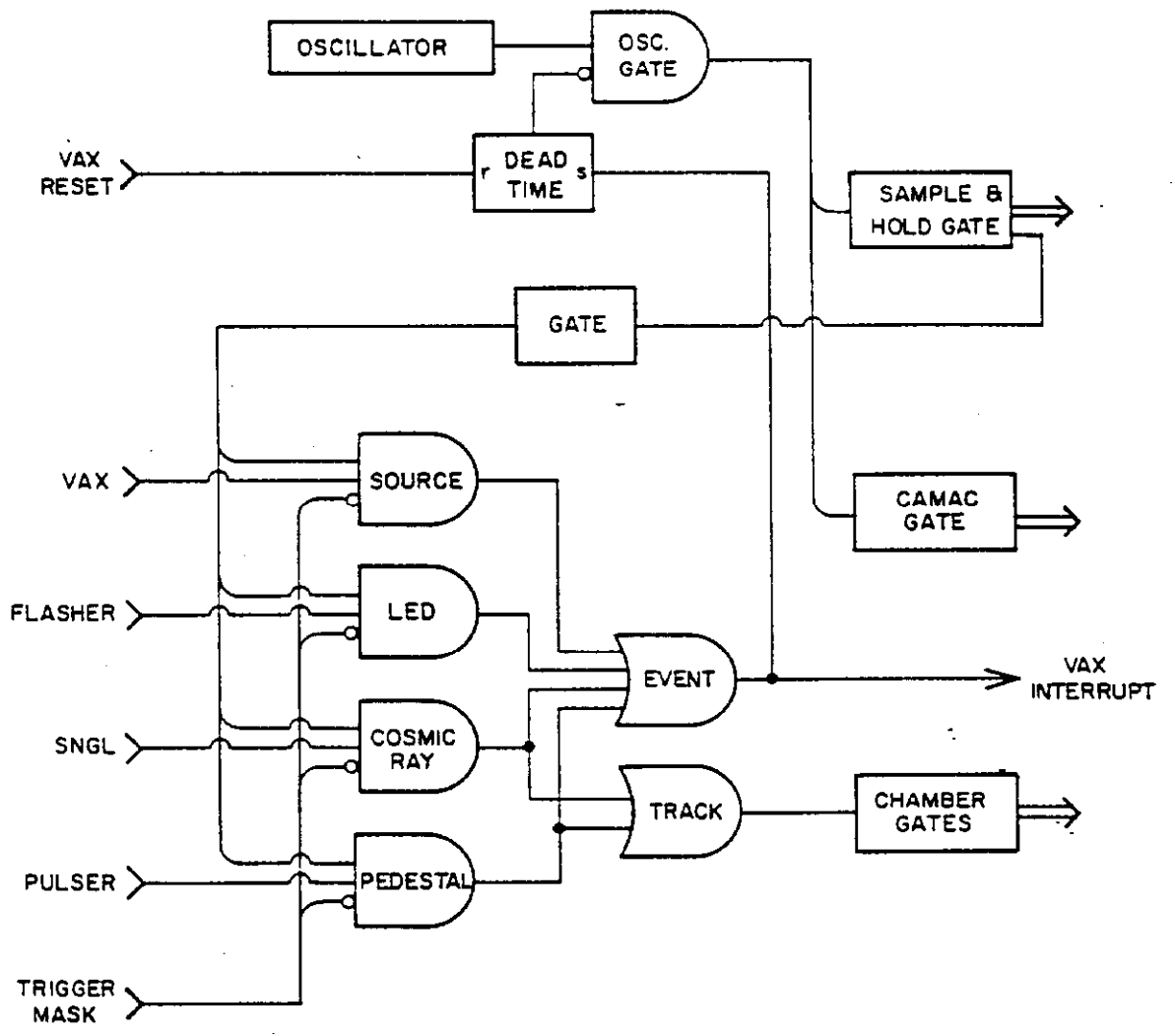


Fig. 4

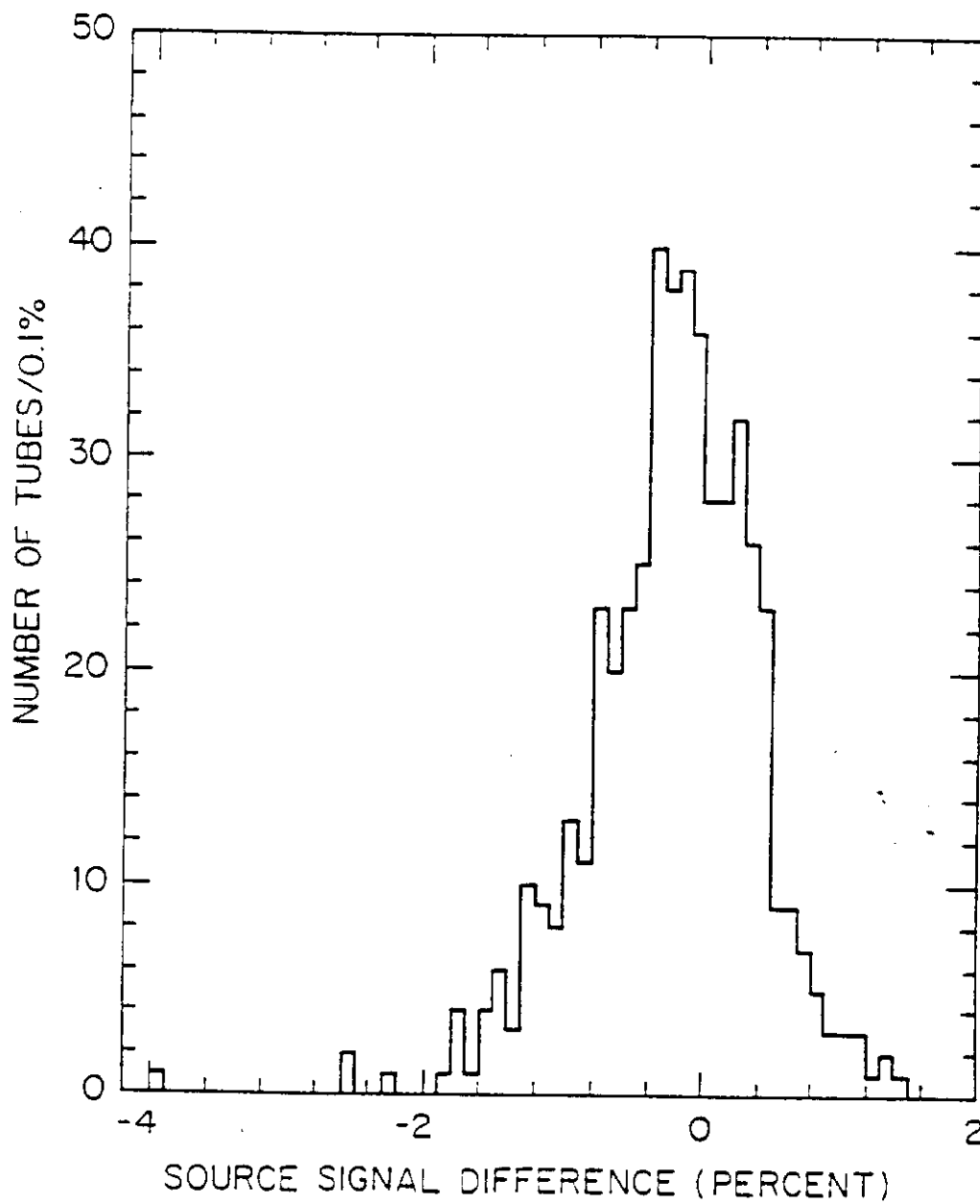


Fig. 5

PHOTOTUBE CHARGE INTEGRATOR GAIN STABILITY

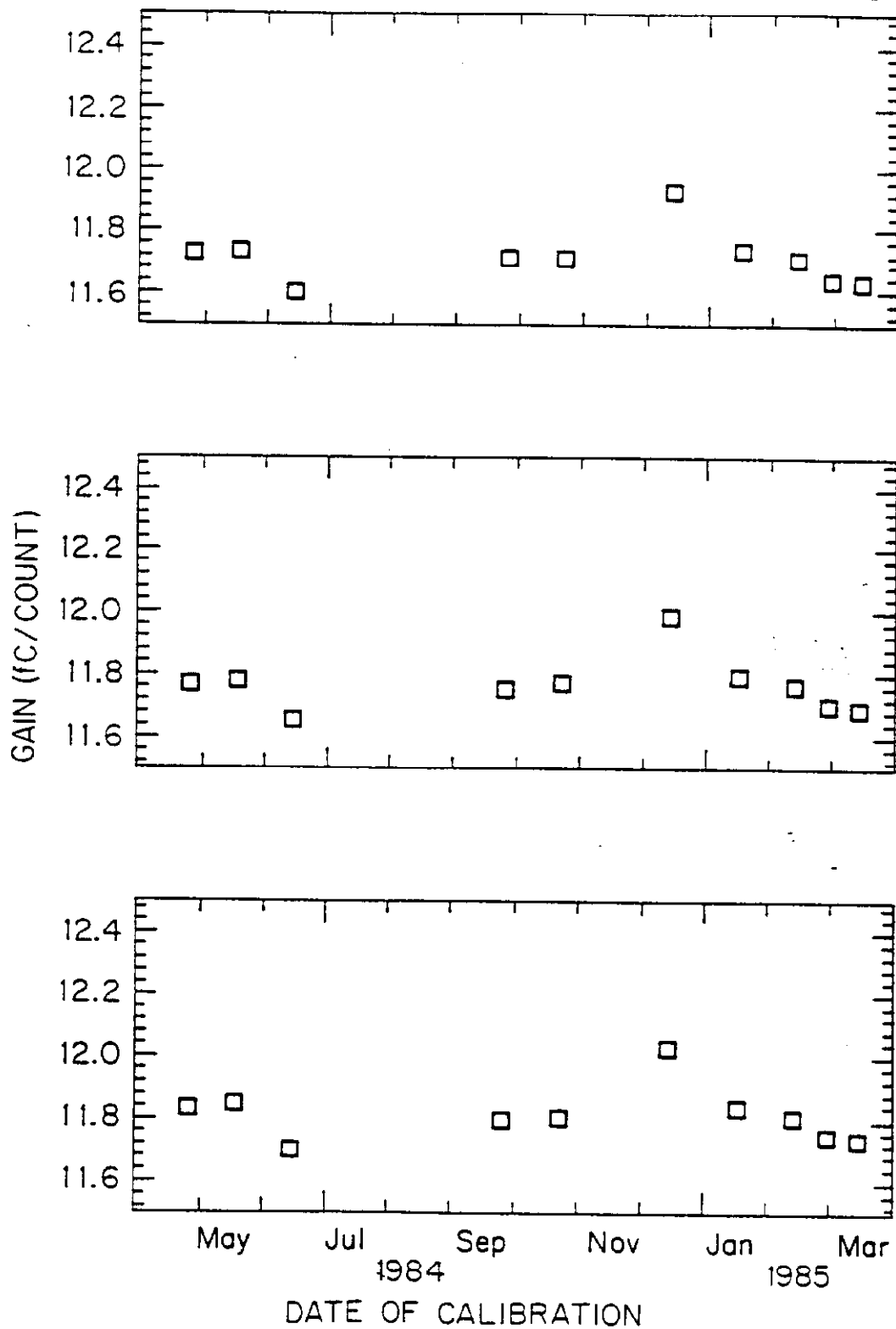


Fig. 6 (a)

PHOTOTUBE CURRENT CHANNEL GAIN STABILITY

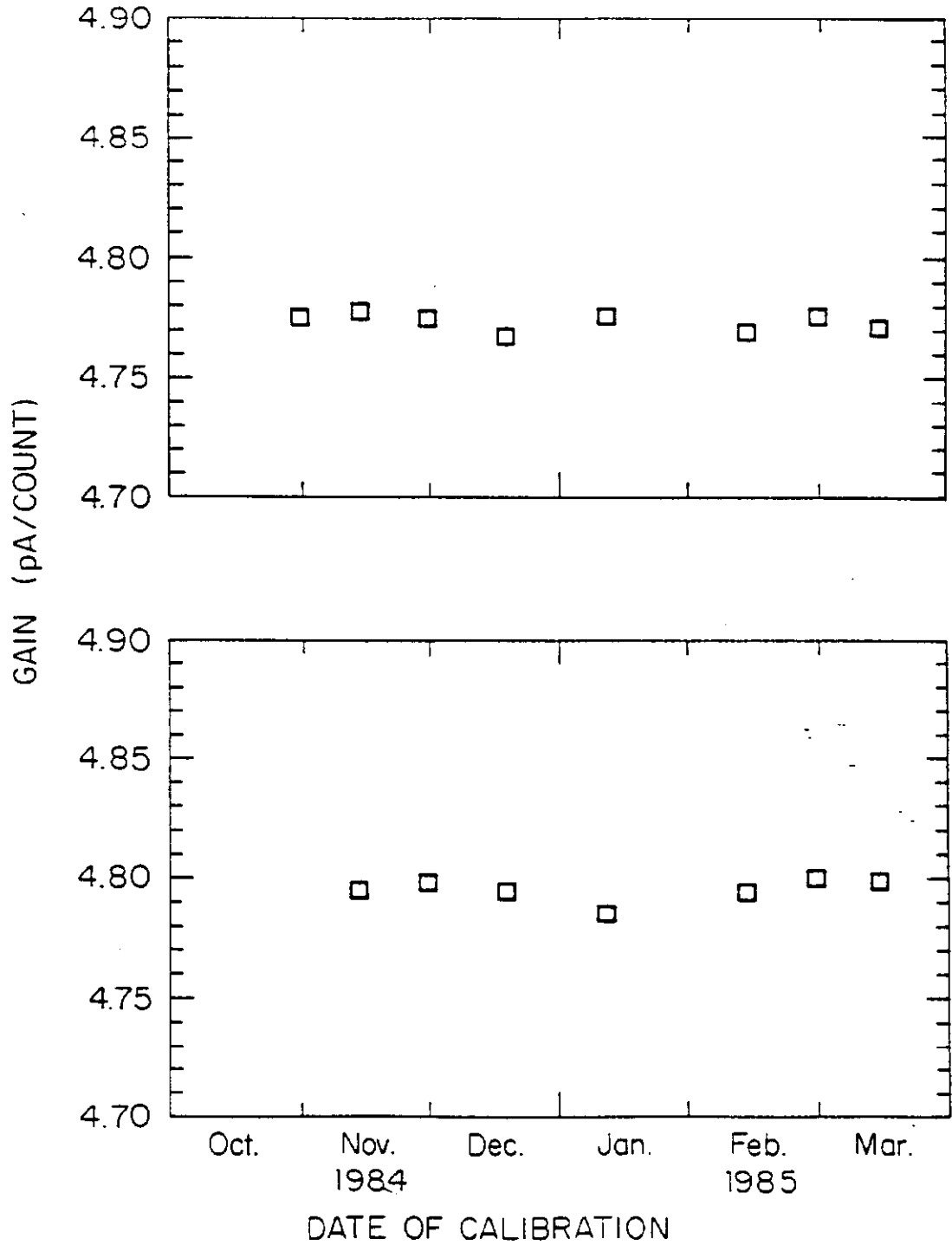


Fig. 6 (b)

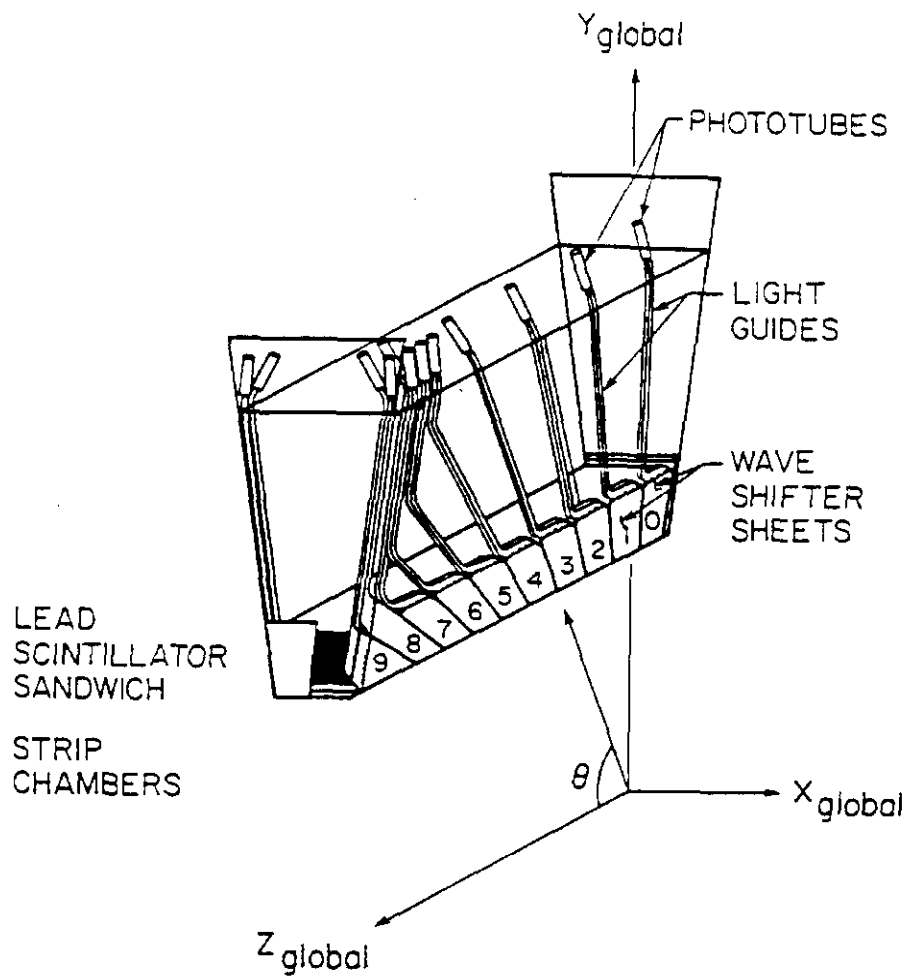


Fig. 7 (a)

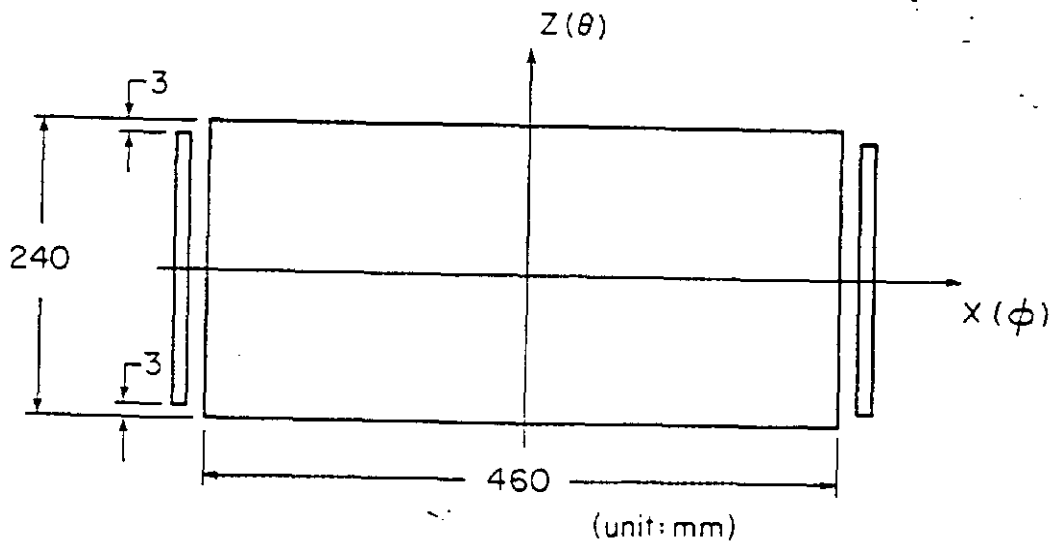


Fig. 7 (b)

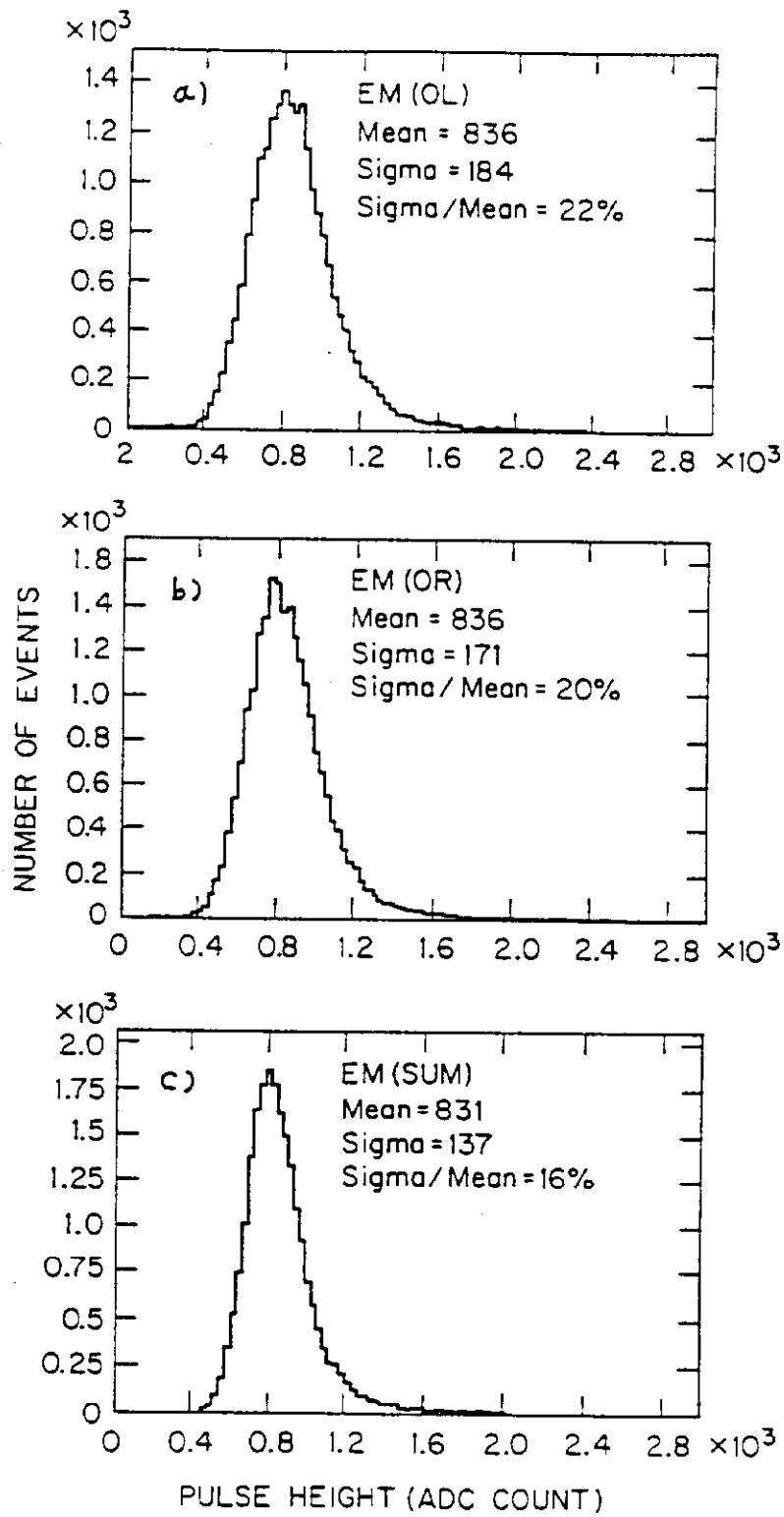


Fig. 8

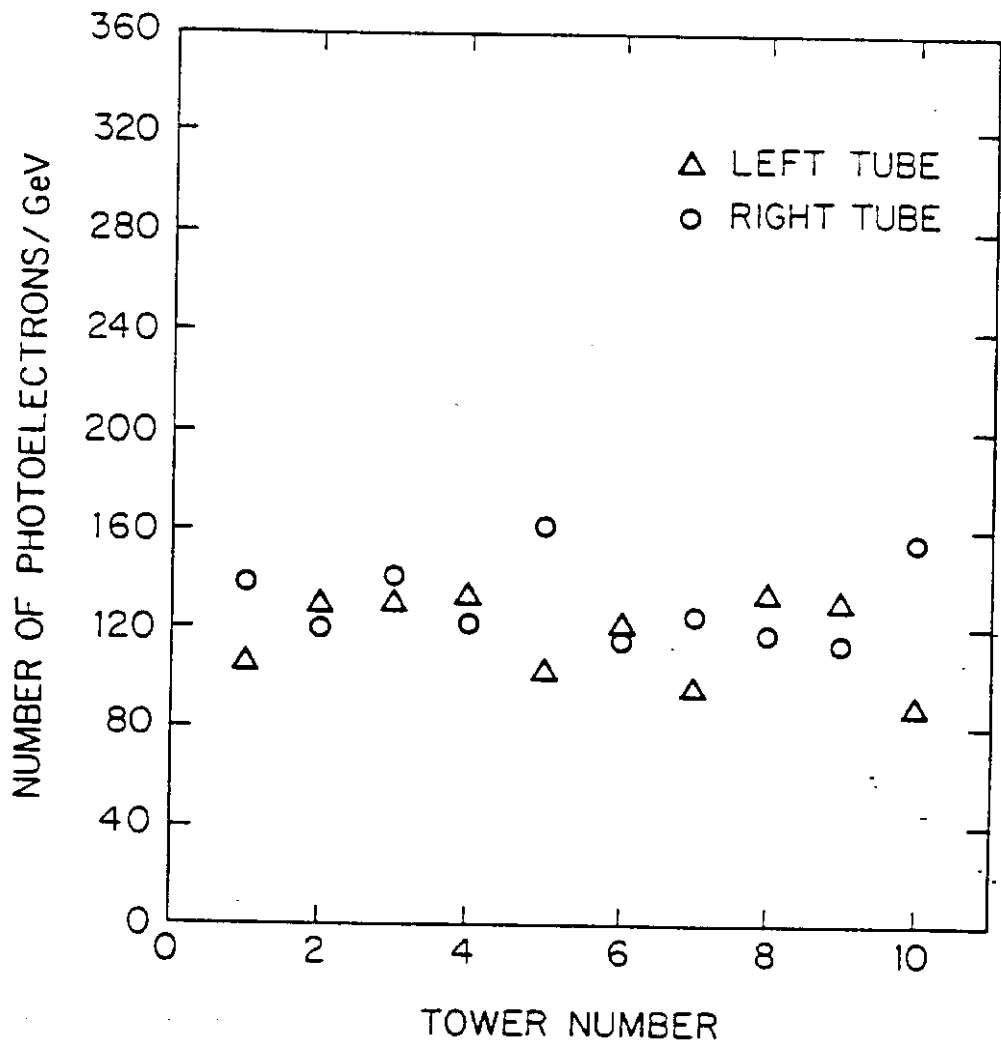


Fig. 9

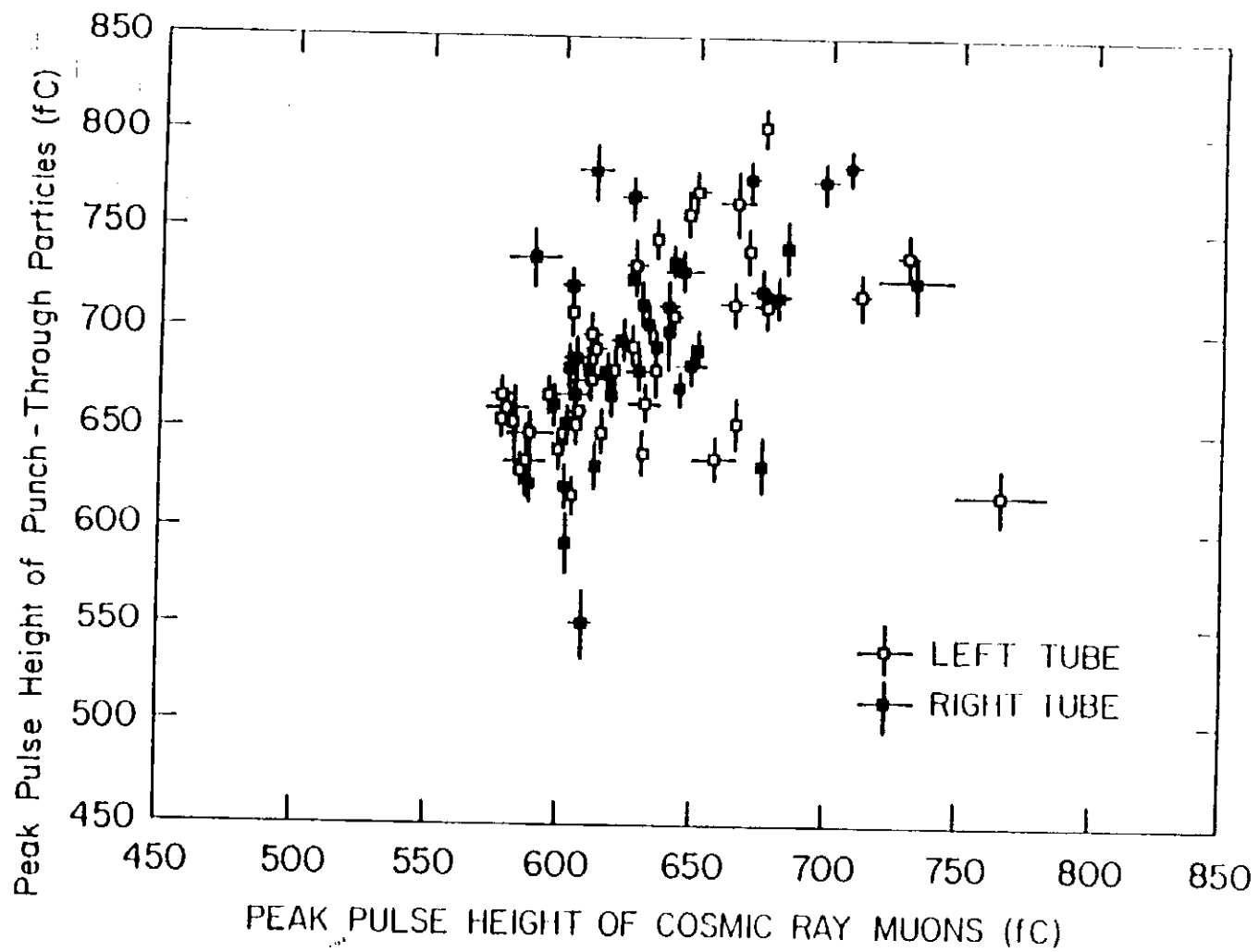


Fig. 10

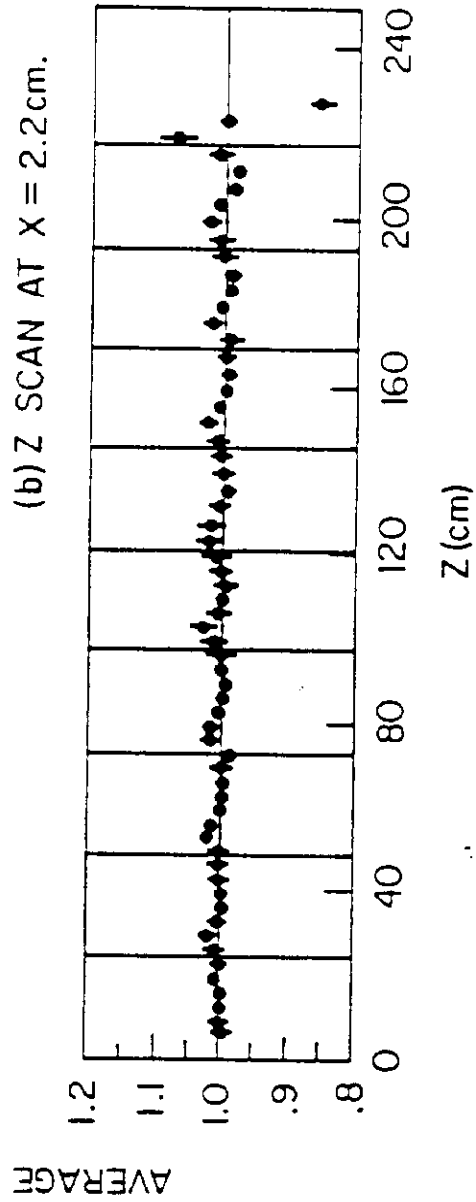
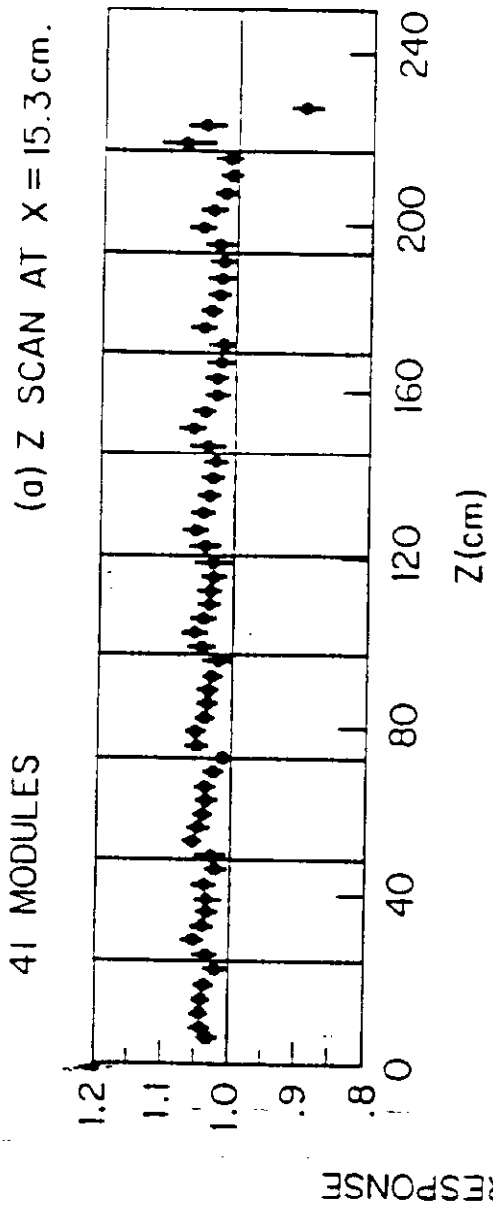


Fig. 11

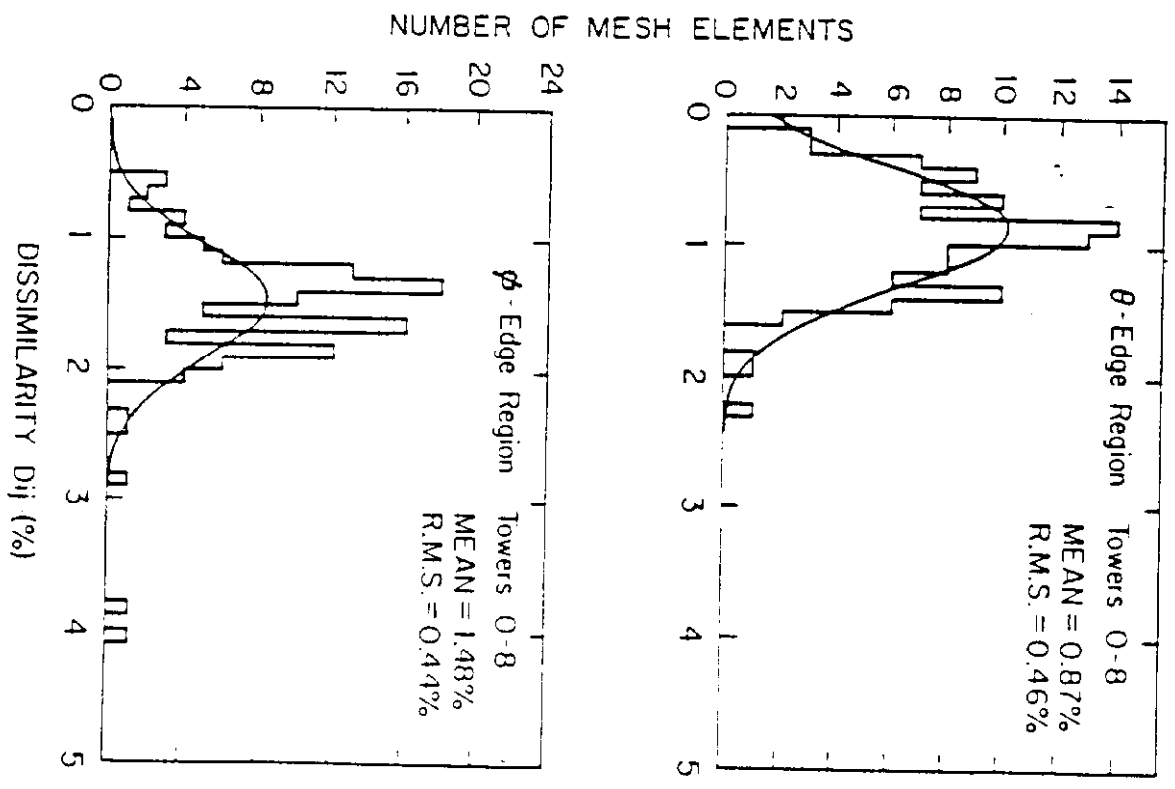
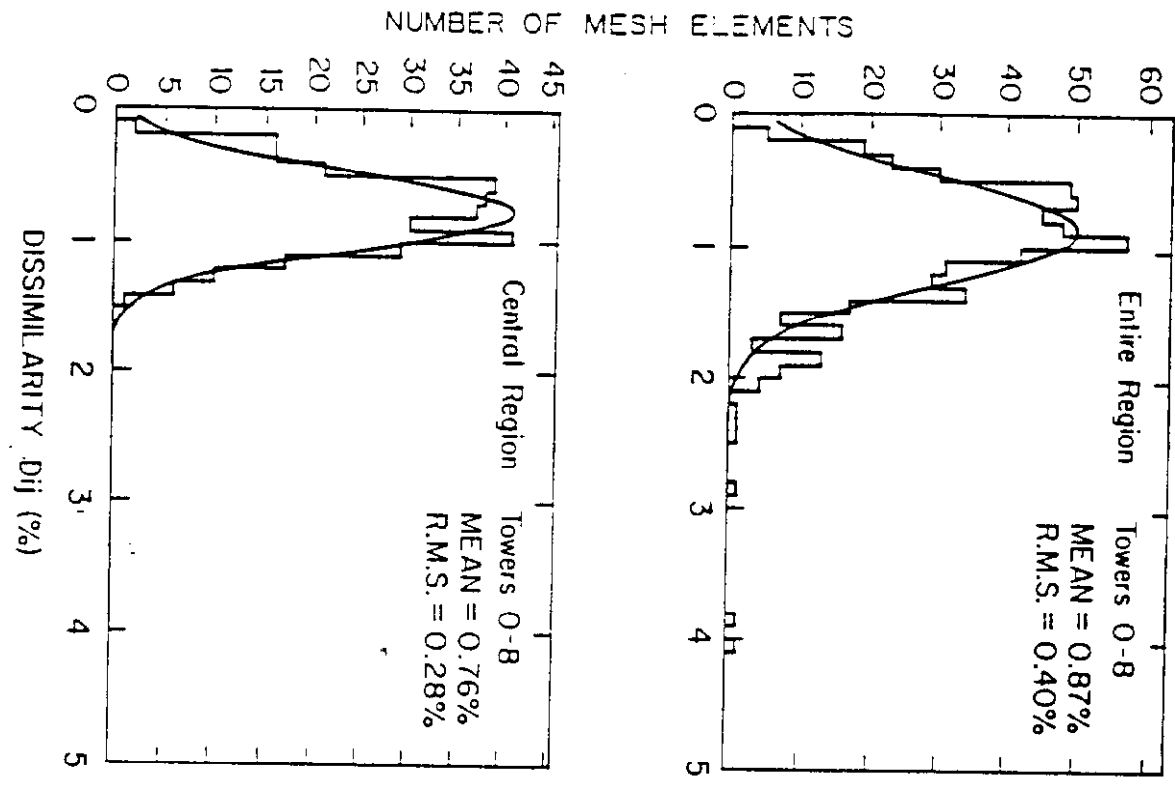


Fig. 12

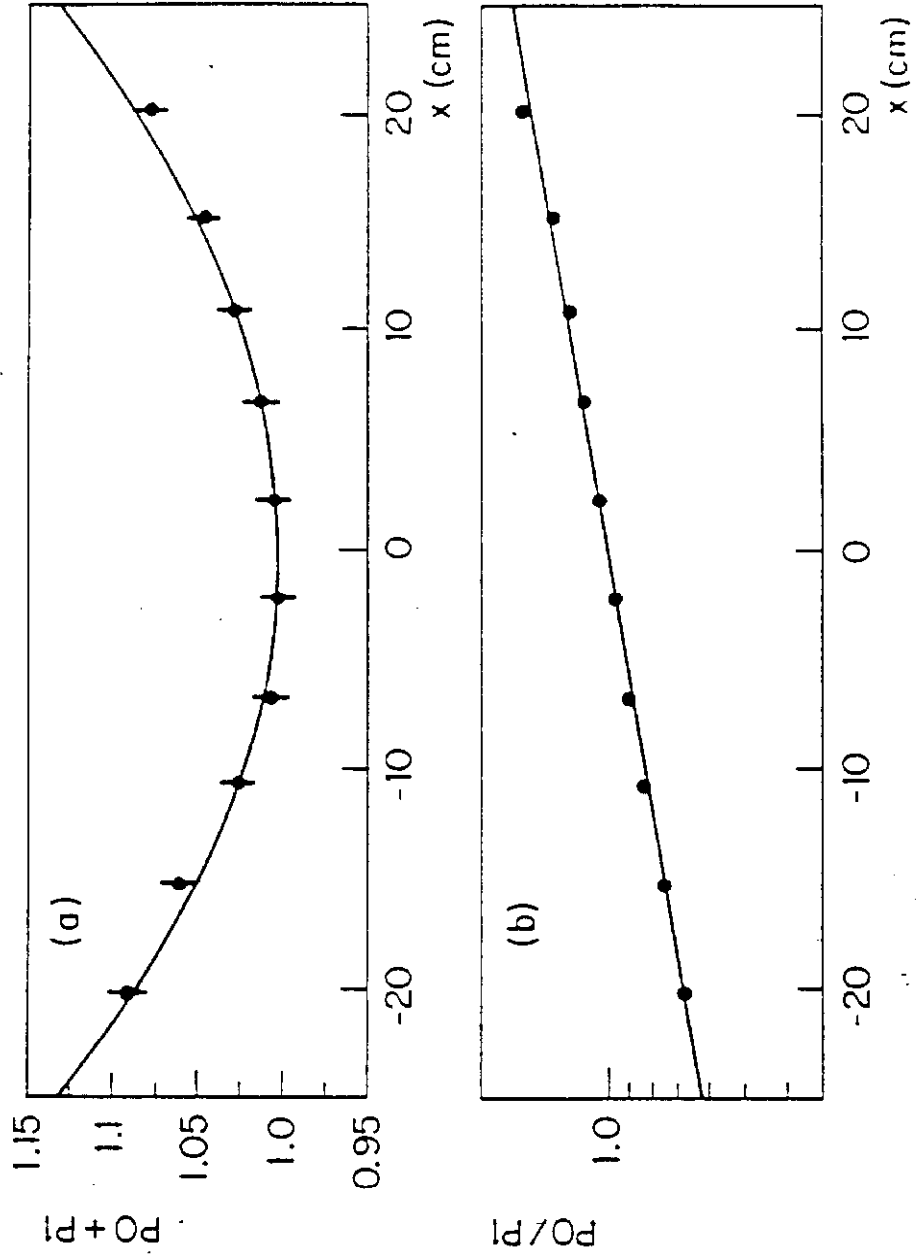


Fig. 13

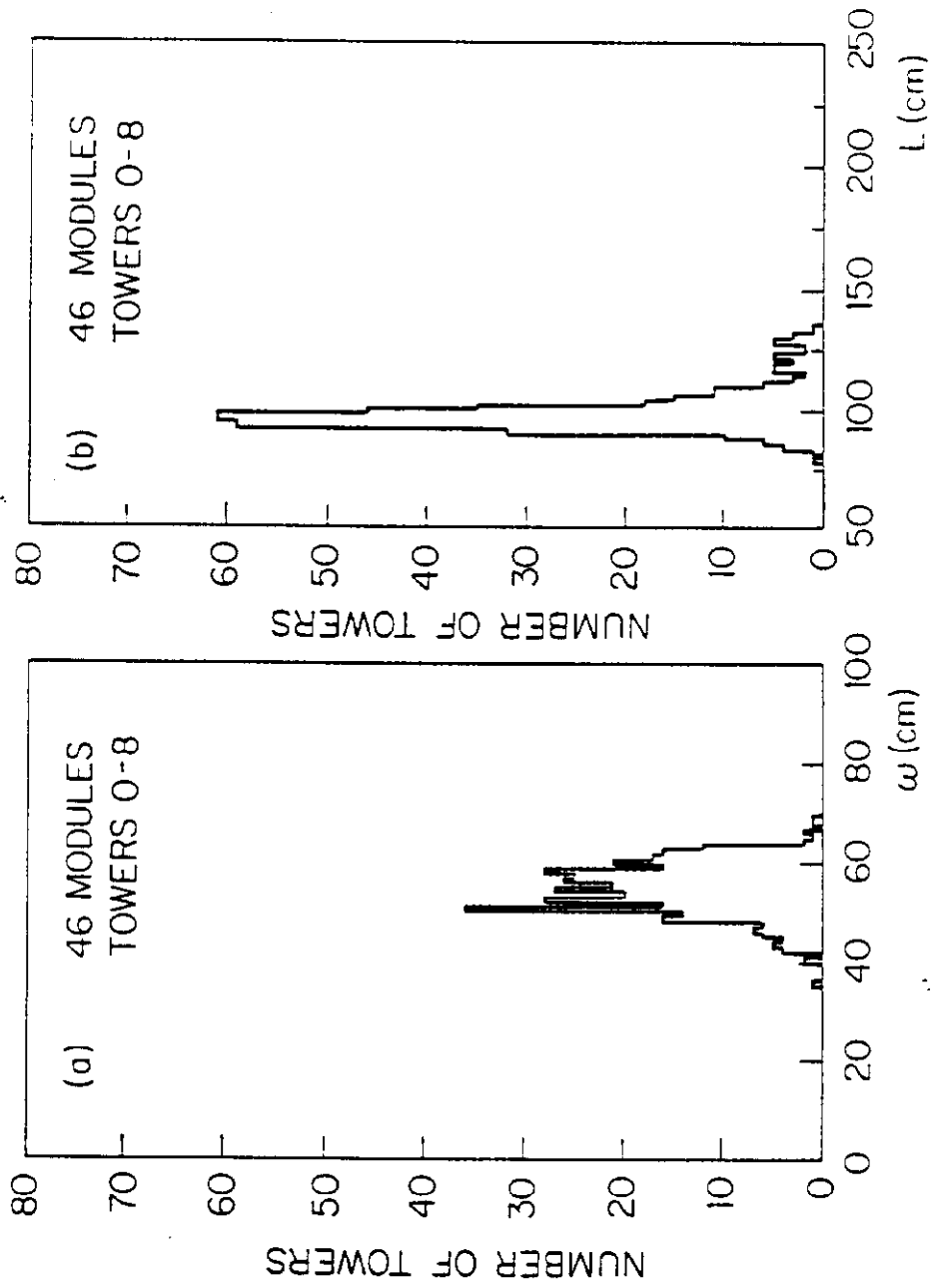


Fig. 14

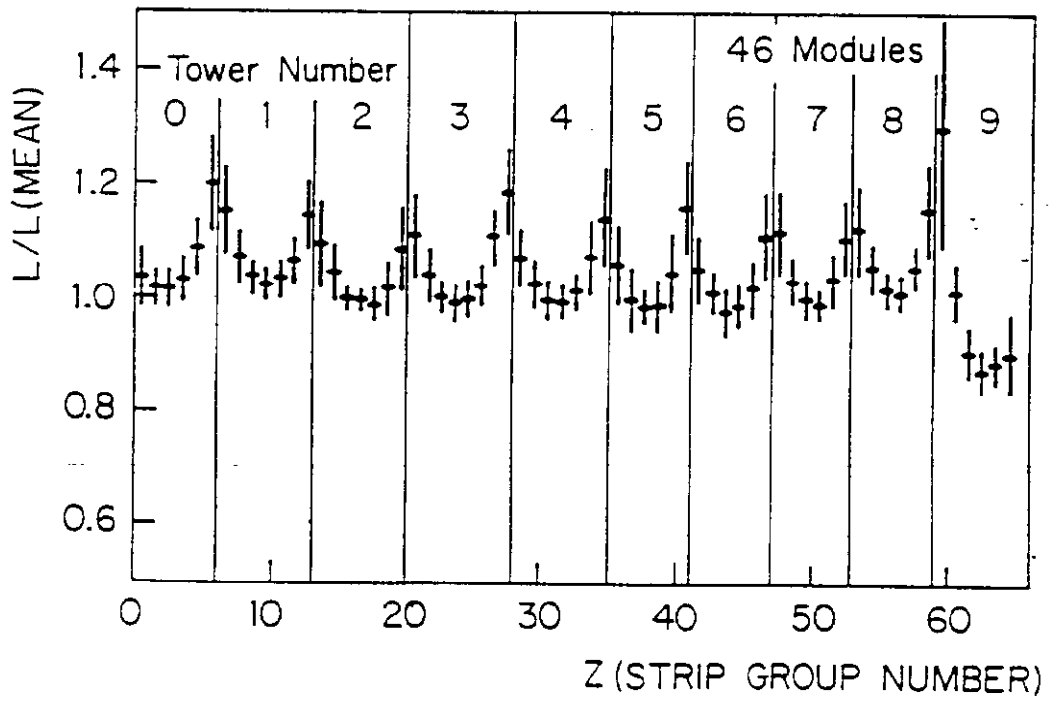
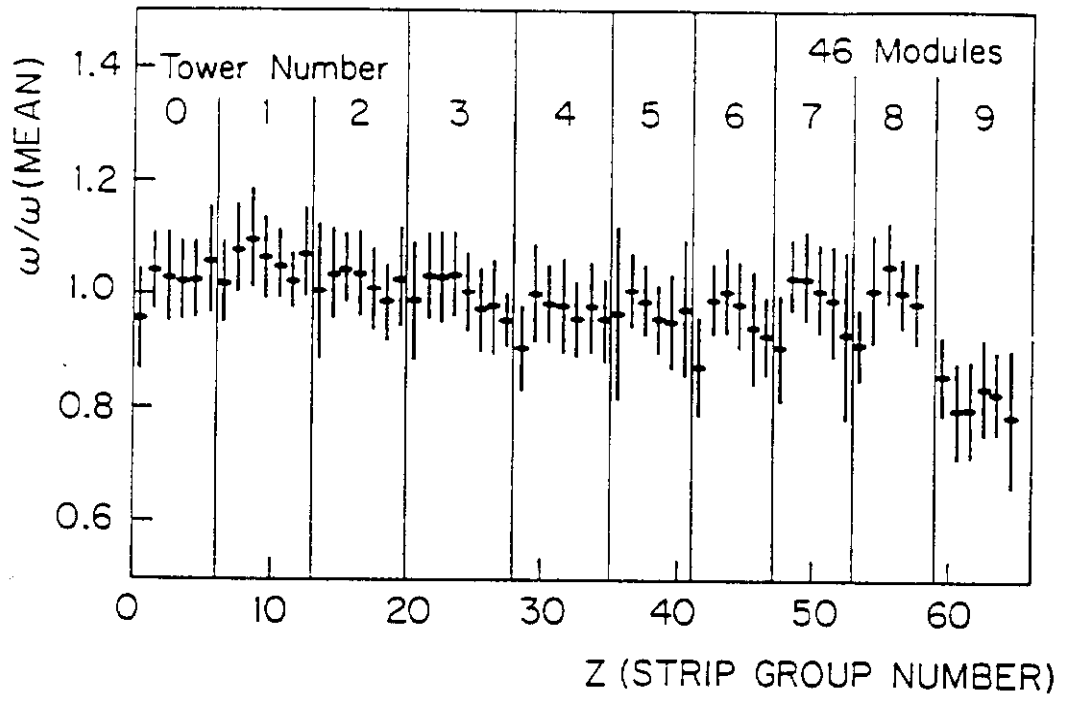


Fig. 15

### Z Dependence of L

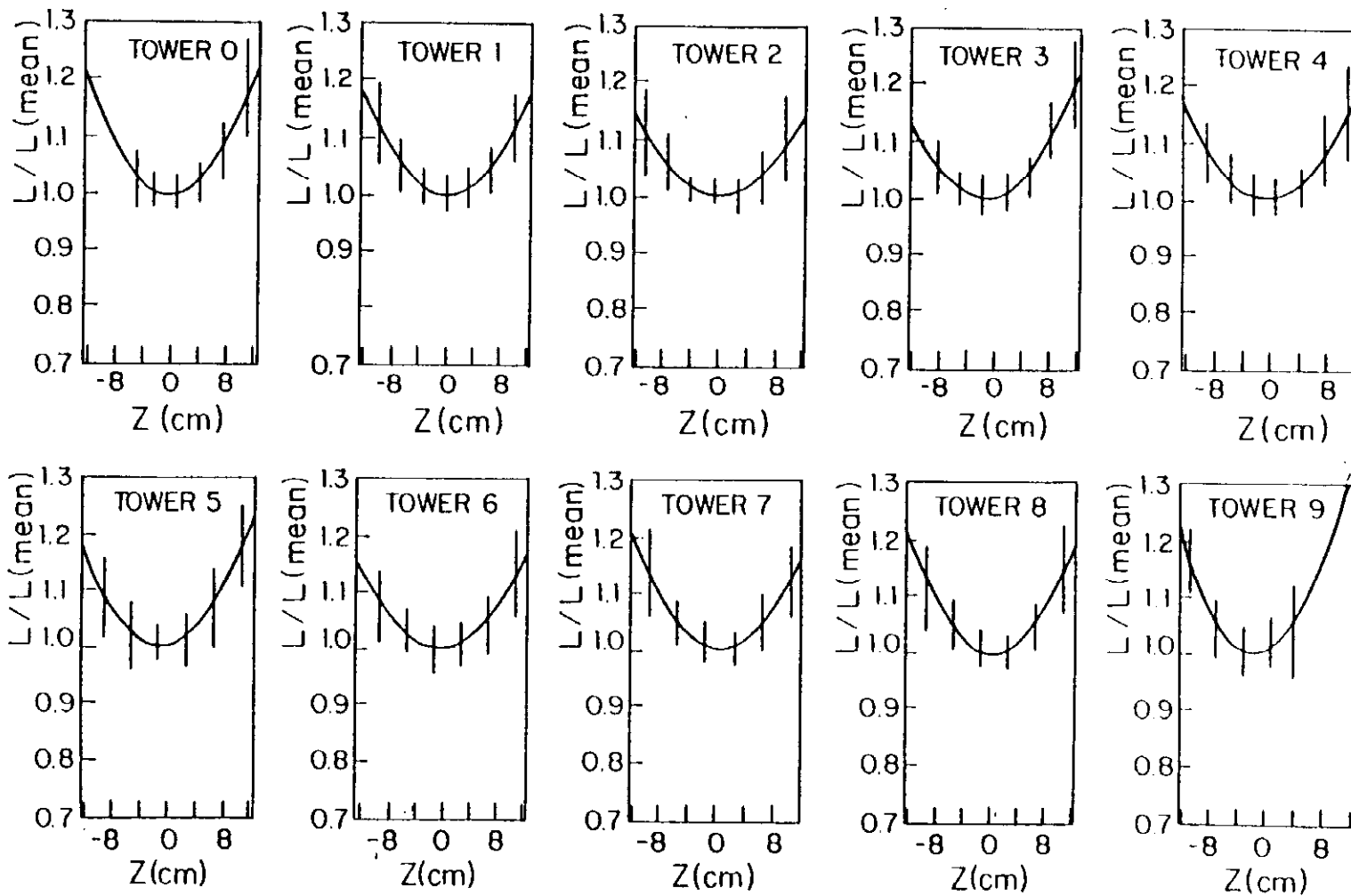


Fig. 16

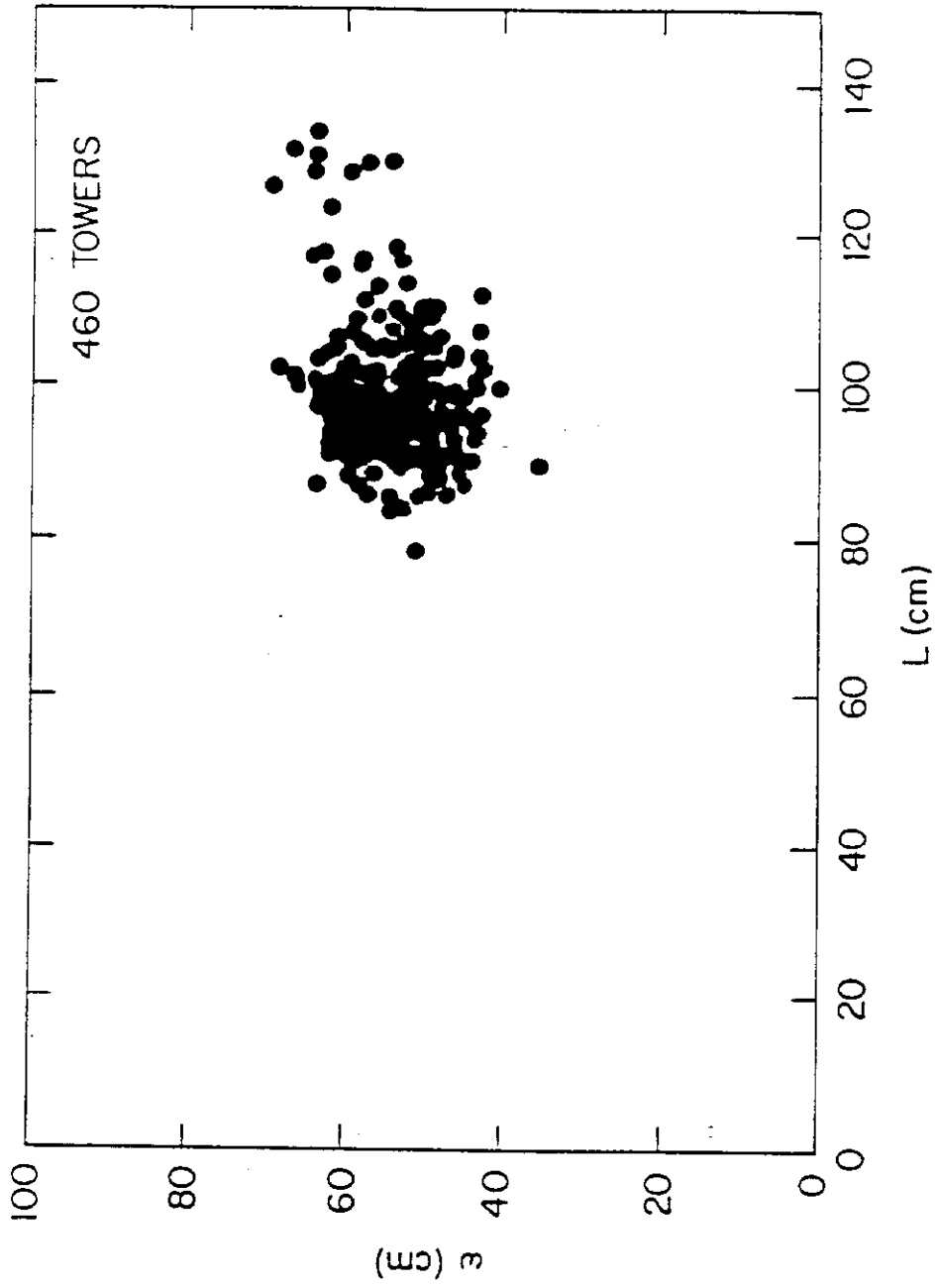


Fig. 17

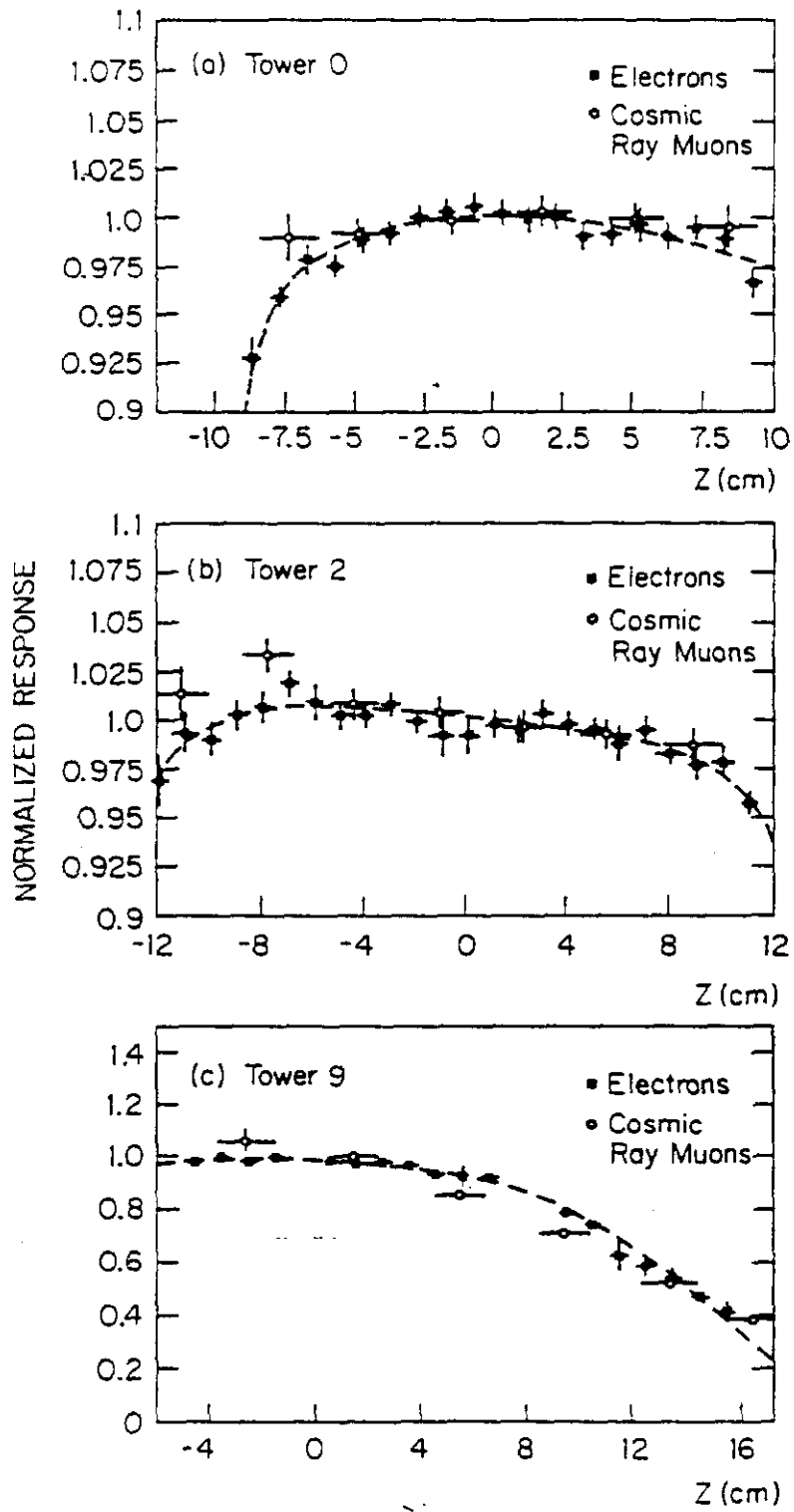


Fig. 18

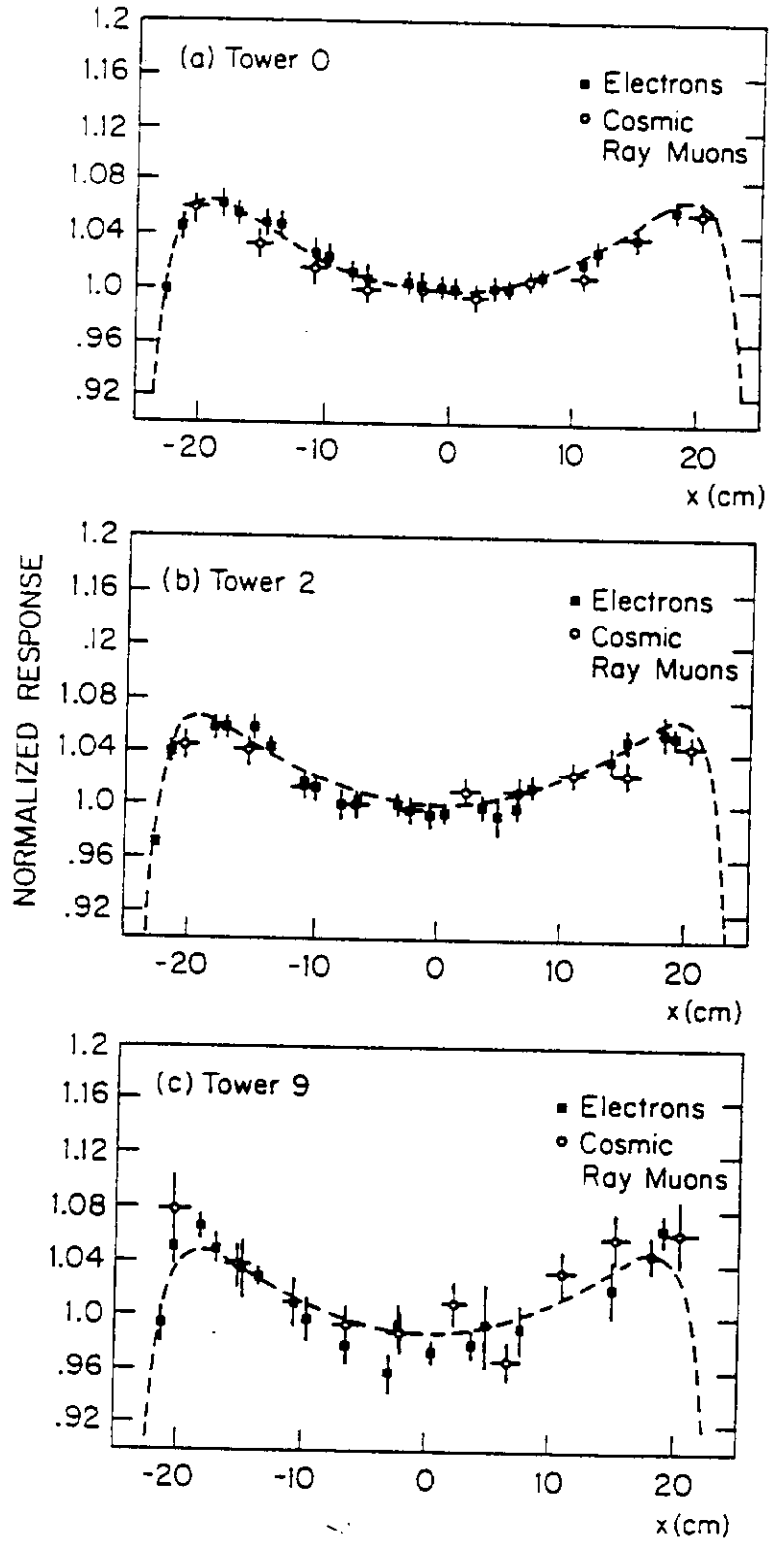


Fig. 19

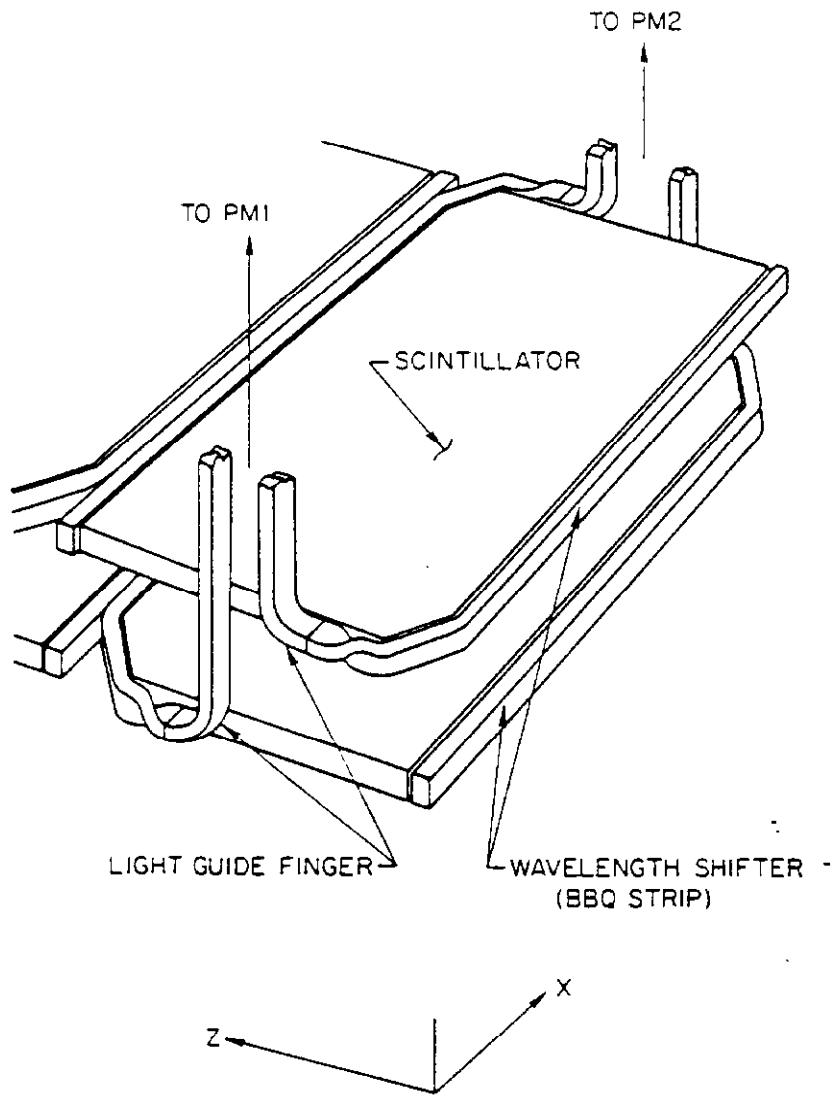


Fig. 20

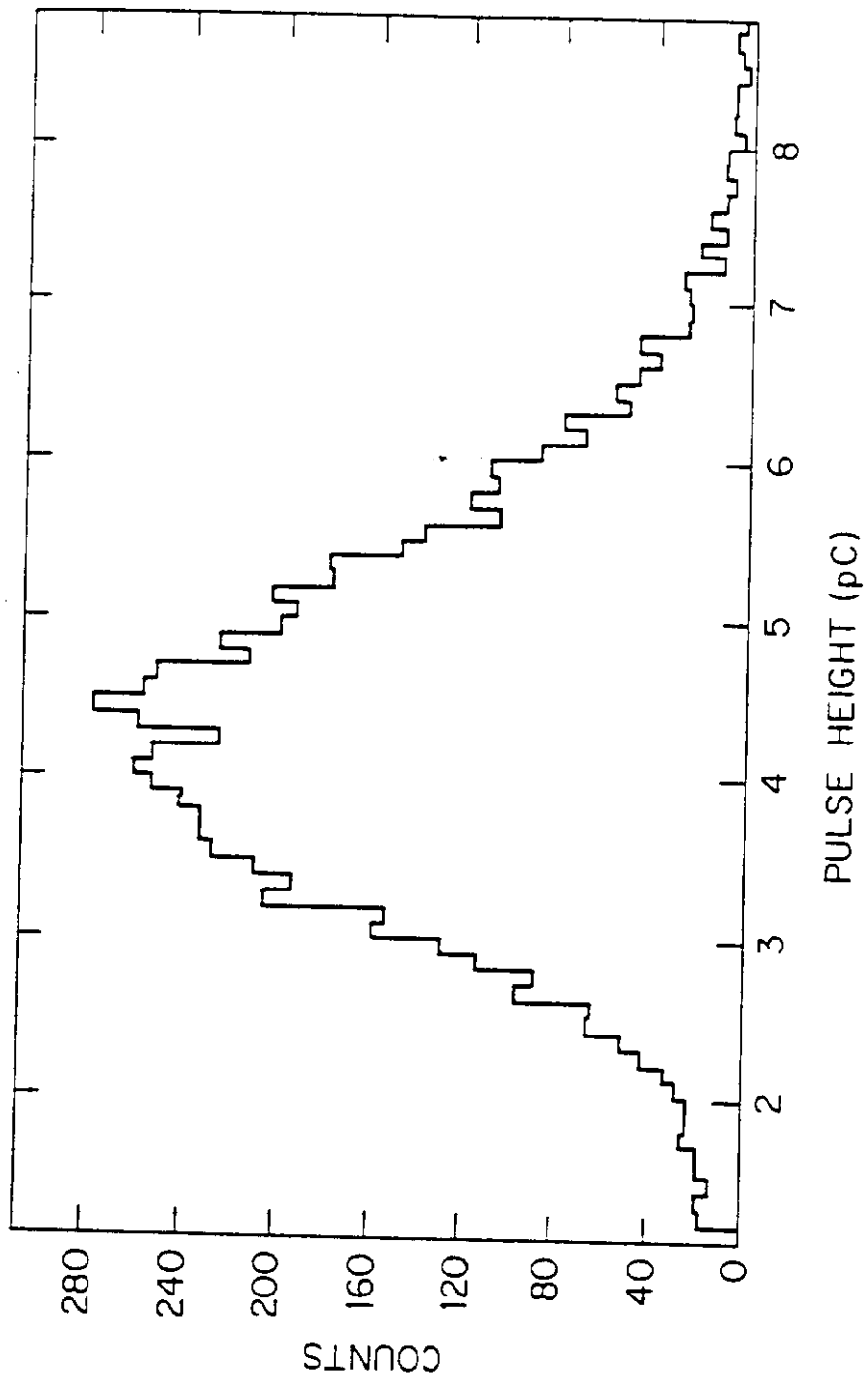
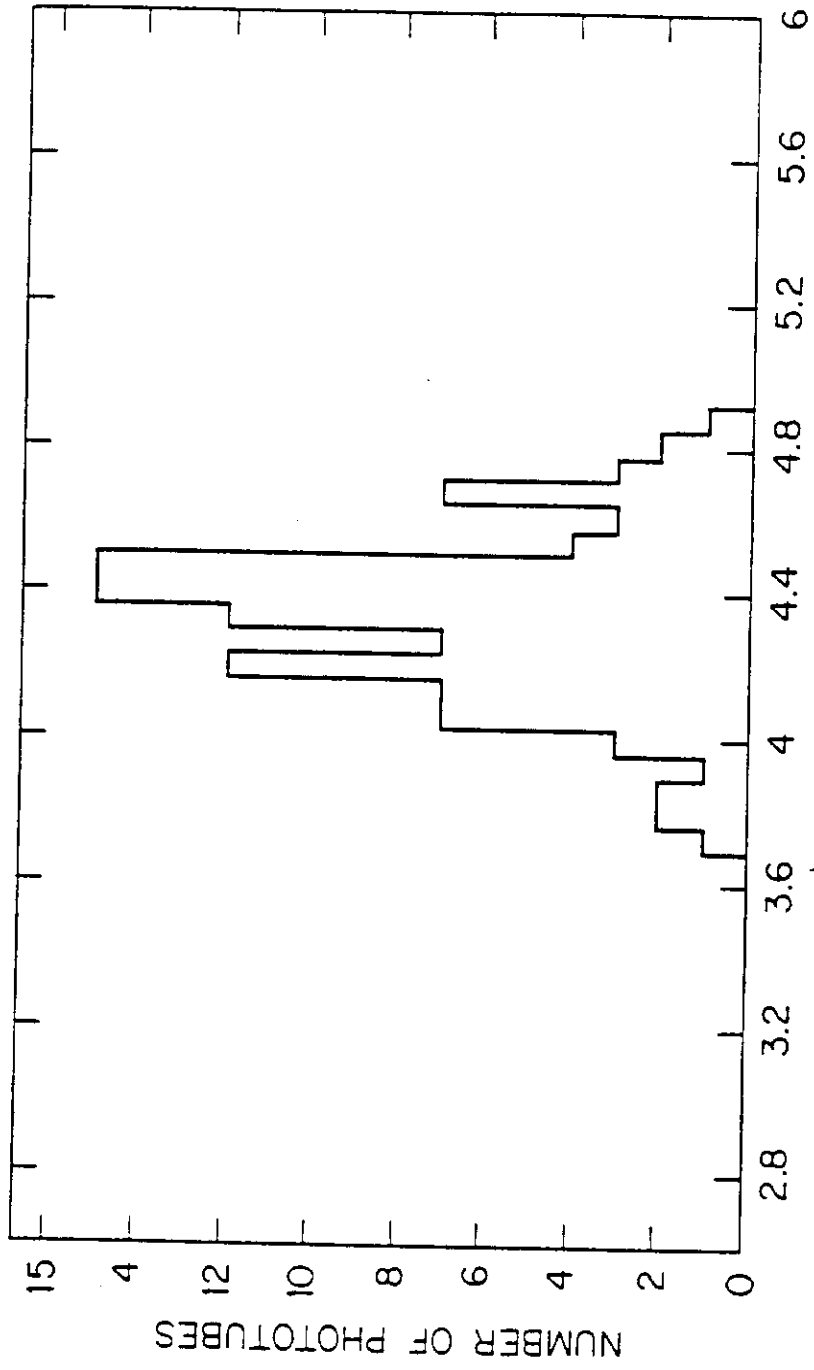


Fig. 21



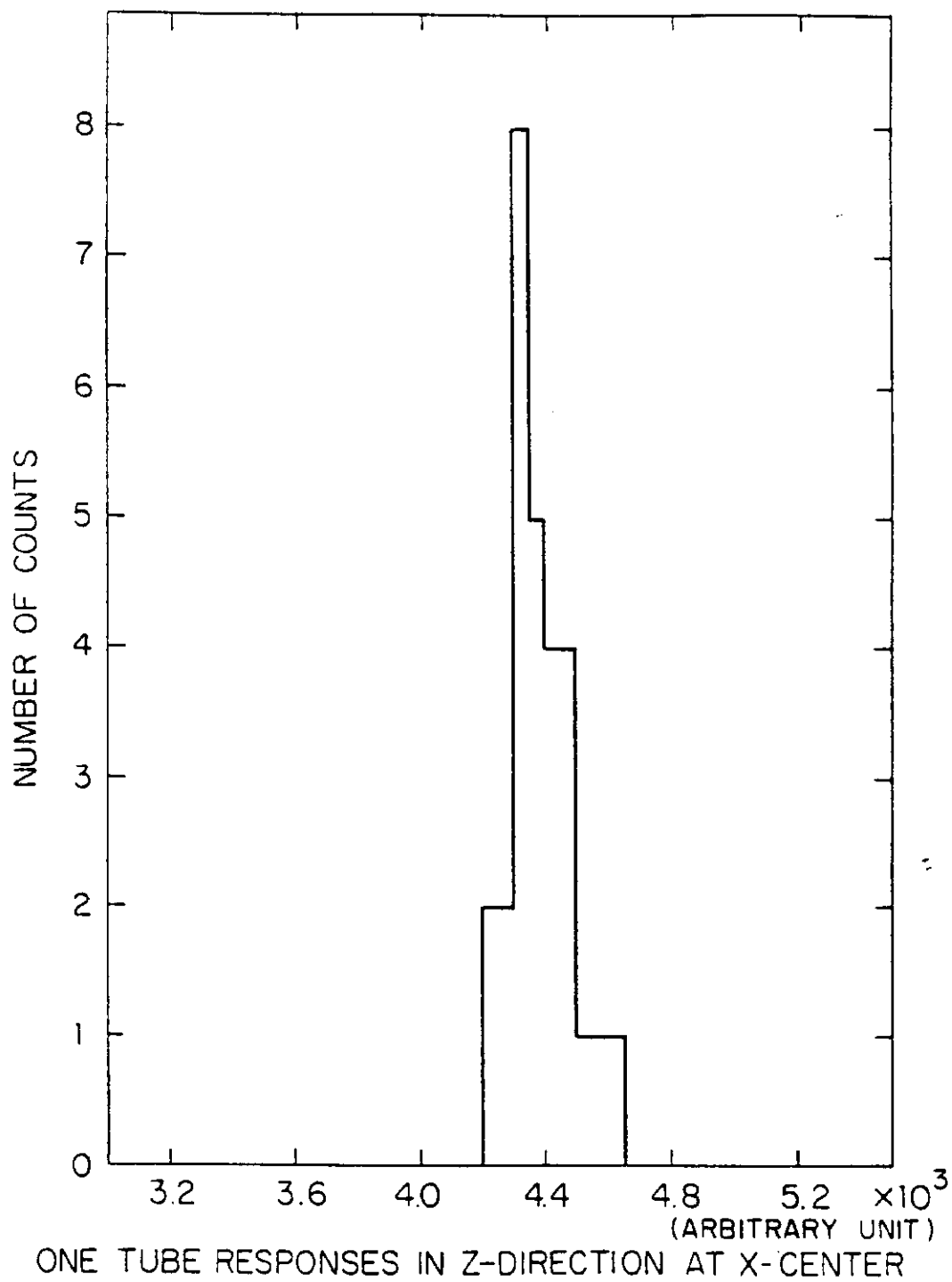


Fig. 23

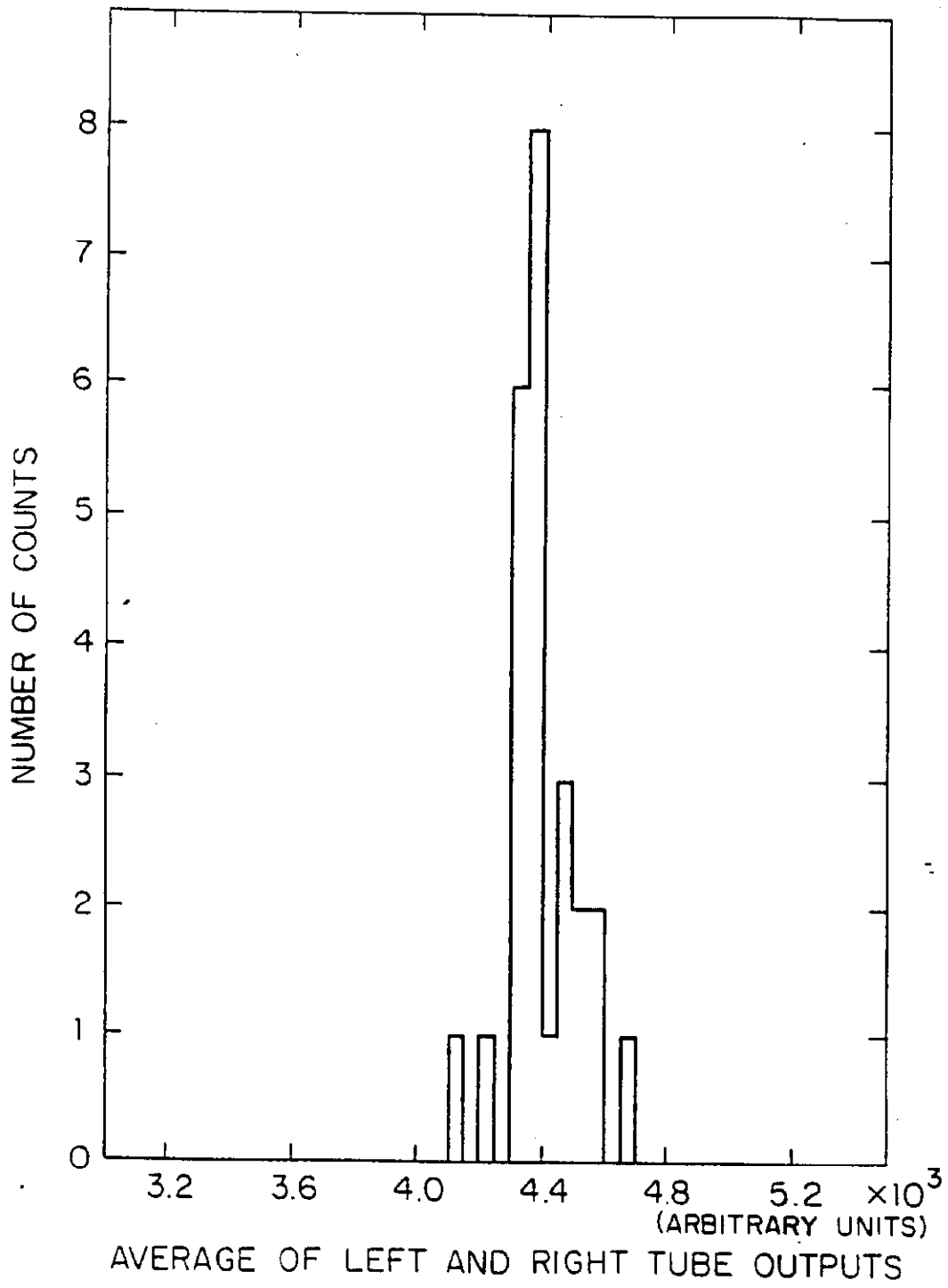


Fig. 24